COPY NO. C 8
RM No. E6L13

RESEARCH MEMORANDUM

INVESTIGATION OF SHOCK DIFFUSERS AT MACH NUMBER 1.85

II - PROJECTING DOUBLE-SHOCK CONES

By W. E. Moeckel, J. F. Connors, and A. H. Schroeder

Flight Propulsion Research Laboratory
Cleveland, Ohio

NATIONAL ADVISORY COMMITTEE
FOR AERONAUTICS

WASHINGTON

June 17, 1947

NATIONAL ADVISORY COMMITTEE FOR AERONAUTICS

RESEARCH MEMORANDUM

INVESTIGATION OF SHOCK DIFFUSERS AT MACH NUMBER 1.85

II - PROJECTING DOUBLE-SHOCK CONES

By W. E. Moeckel, J. F. Connors, and A. H. Schroeder

SUMMARY

An investigation has been undertaken in the Cleveland 18- by 18-inch supersonic tunnel to determine the total-pressure recovery obtainable at a Mach number of 1.85 with a shock diffuser having projecting cones designed to produce two oblique shocks ahead of the diffuser inlet. The variation of total-pressure recovery with tip projection was investigated for each of four cones with different included angles. Each cone was investigated with a straight and with a curved diffuser-inlet section. The effect of angle of attack and the distribution of static and total pressures at the diffuser outlet were also investigated for the best configurations.

A maximum total-pressure recovery of 94.5 percent was attained with the best configuration at an angle of attack of 0°. At an angle of attack of 5°, this maximum recovery was reduced to 89.9 percent. These total-pressure recoveries correspond to efficiencies of kinetic-energy conversion of 97.6 percent at 0° and 95.5 percent at 5° angle of attack. Several other configurations gave maximum total-pressure recoveries greater than 93.0 percent at an angle of attack of 0°.

With each cone, three oblique shocks appeared ahead of the diffuser inlet instead of the two theoretically predicted. The additional oblique shock resulted from a bridging of the break in the cone surface by the boundary layer.

The highest total-pressure recoveries were obtained with subsonic inlet flow. For outlet areas less than optimum, the total-pressure recovery dropped to values lower than those obtained with single-shock cones.

INTRODUCTION

An investigation of shock diffusers at a Mach number of 1.85 is being conducted in the Cleveland 18- by 18-inch supersonic tunnel. Results obtained with a shock diffuser having a single oblique shock

ahead of the inlet are presented in reference 1 and are compared with theoretically estimated results. A maximum total-pressure recovery of 92.2 percent was attained.

When the projecting cone is designed with an abrupt increase in the included angle at some distance from the tip, a second oblique shock should arise from the break in the contour. A higher total-pressure recovery should be obtainable with two shocks ahead of the inlet because the total-pressure ratio for a given reduction in Mach number is greater across two oblique shocks than across one.

Four cones having abrupt increases in included angle at some distance from the tip were designed for investigation in the diffuser body of reference 1. Each of these cones was used in combination with a straight and with a curved inlet to determine whether higher total-pressure recoveries were obtainable with abrupt or gradual deflection of the entering flow. The total-pressure recovery was determined for each cone-inlet combination as a function of tip projection and outlet area. The effect of angle of attack and the pressure distributions at 0° and 5° angle of attack were determined for the best configurations.

APPARATUS AND PROCEDURE

Diagrams of the test model, which is the same as that used in the investigation of single-shock cones (reference 1), are shown in figure 1. A conical damper at the outlet of the simulated combustion chamber was used to vary the outlet area. Pressures at the diffuser outlet for various values of outlet area were obtained with a pitot-static rake located as shown in figure 1(a). Total-pressure recoveries were measured for a series of tip projections varied in minimum steps of one-sixteenth inch. Because construction of a theoretically correct inlet for each cone and tip projection was not expedient, the cones were tested only with the straight and with the curved inlets of reference 1.

The four cones investigated and the theoretical location of the oblique shocks at minimum tip projection are shown in figure 2. The second shock was approximately determined from oblique-shock theory by assuming a constant flow deflection through the shock. The break in each cone is located 1 inch from its tip. These cones are designated 20-40, 30-50, 30-60, and 40-70 according to their included angles ahead of and after the break (fig. 2). The bow wave that occurs at the inlet for all except the 40-70 cone is not shown in figure 2 because its location is not readily determinable.

The tunnel was calibrated from measurements of oblique-shock angles at cone tips and from total-pressure measurements. The Mach number and total pressure in the test section as determined by this method are accurate within about 2 percent. The relative total-pressure recoveries obtained in the investigation, however, are accurate within about 0.5 percent. The Reynolds number at the diffuser, based on the maximum diffuser diameter ($4\frac{1}{8}$ in.), is approximately 1.34×10^6.

SYMBOLS

The following symbols are used (see fig. 3):

A	area
A_i	inlet area with cone removed
L	tip projection, inches
M	Mach number
P	total pressure
p	static pressure
V	velocity
$\theta_{c,1}$	half-angle of cone at tip, degrees
$\theta_{c,2}$	half-angle of cone beyond break, degrees
λ	angle between local and free-stream flow directions, degrees
ρ	density
φ	angle between shock and free-stream direction, degrees
Ψ_1	angle of ray from tip, degrees
Ψ_2	angle of ray from break, degrees

Subscripts:

0	conditions in free stream
1	flow field between first and second oblique shock

2	flow field between second oblique shock and diffuser entrance
3	conditions at minimum area
4	conditions at diffuser outlet
a	conditions immediately behind shock
b	conditions at other points in field behind shock
c	conditions at surface of cone
cr	critical values
e	conditions at diffuser entrance
max	maximum values

THEORY

Theoretical predictions of the performance of shock diffusers are more difficult for double-shock than for single-shock cones. The velocity distribution ahead of the second shock is not uniform and consequently the second shock is, in general, curved and of varying intensity. (See fig. 3.) Numerical methods of finding the form of the second shock and the velocity distribution in the field behind it have been developed but are quite laborious (reference 2). It is therefore of interest to determine how closely the entrance conditions may be approximated by making certain simplifying assumptions.

The procedure whereby approximate values of the entrance Mach number M_e were obtained is as follows (fig. 3): The angle of the first shock φ_1, the Mach number behind it $M_{1,a}$, and the Mach number at the cone surface $M_{1,c}$ were known from oblique-shock theory and from conical-flow theory. The angle of flow deflection $\lambda_{1,a}$ through the first shock is also known. The variation of flow direction λ_1 and the distribution of Mach number in the field between the first shock and the cone surface were determined by assuming a linear variation of these quantities with the angle of a ray from the cone tip Ψ_1.

In order to continue the approximation, the form of the second shock arising from the break in the cone surface had to be determined. Schlieren photographs showed that two oblique shocks, rather than one,

occurred near the break; the first originated slightly ahead of the break and the other slightly beyond it. A theoretical shock, whose location coincided approximately with the average location of the two observed shocks, was obtained by assuming that the deflection of the flow was constant through the shock at each point. With the Mach-number distribution and the variation of flow direction ahead of this theoretical shock known, the shock angle at each point was determinable from oblique-shock relations.

The approximate location of the oblique shocks for minimum tip projection, as determined in this manner, is shown for each cone in figure 2. For the inlets used, a bow wave (not shown) occurs ahead of the inlet for all except the 40-70 cone at minimum tip projection. The form and location of this bow wave are not readily determinable. For the 40-70 cone, the angle of deflection of the flow through the second shock was great enough to produce subsonic velocities everywhere behind the second shock. Although the shock may still be oblique to the flow for such cases, φ_2 and M_2 are no longer determinable from oblique-shock relations. Because the theoretical total-pressure recoveries are the same whether M_e is assumed to be sonic or subsonic, the value of M_e for the 40-70 cone was assumed to be equal to 1.0 throughout the calculations.

For the other three cones, however, M_e was taken as the average of the Mach number at the cone surface beyond the break $M_{2,c}$ and the Mach number at the entrance lip $M_{2,b}$. A linear variation of Mach number with the angle of a ray from the break in the cone Ψ_2 was assumed to determine $M_{2,b}$. The estimated variation of M_e with tip projection is shown in figure 4 for each cone-inlet combination. The ratio of the entrance flow area A_e to the throat area A_3 (fig. 4) was determined, as in reference 1, by assuming that A_e is normal to the cone surface.

The theoretical variation of total-pressure recovery with outlet area, as stated in reference 1, falls into two distinct regions: the subcritical and the supercritical. In the subcritical region, where the normal shock remains outside the diffuser inlet and the mass flow varies with outlet area A_4, the total-pressure recovery with certain simplifying assumptions (see reference 1) is equal to the product of the total-pressure ratios across the two oblique shocks and across the normal shock occurring at Mach number M_e. The total-pressure ratio across the first oblique shock is readily obtained from conical-flow theory. Across the second oblique shock, however, the total-pressure ratio may vary from point to point. The value assumed

throughout this paper is the total-pressure ratio at the cone surface, which is determined from the flow deflection at the surface $\theta_{c,2} - \theta_{c,1}$ and from the Mach number ahead of the shock $M_{1,c}$.

In the supercritical region, where the mass flow remains constant as A_4 is varied, the relation between total-pressure recovery and outlet area is given by the equation (reference 1):

$$\frac{P_4 A_4}{P_0 A_1} = \frac{(\rho V)_0 A_0}{(\rho V)_{0,cr} A_1} \tag{1}$$

where the ratio $(\rho V)_0/(\rho V)_{0,cr}$ is equal to 0.669 at a Mach number of 1.85. The method used in reference 1 for approximating the free-stream flow area A_0 (that is, sketching the limiting streamline of the entering flow) was not used because with two oblique shocks the inaccuracy of the method resulted in disagreement with experimental results. An equivalent form of equation (1) that uses A_e rather than A_0 was therefore used:

$$\frac{P_4 A_4}{P_0 A_1} = \frac{(\rho V)_e}{(\rho V)_{e,cr}} \frac{P_e}{P_0} \frac{A_e}{A_1} \tag{2}$$

where $(\rho V)_e/(\rho V)_{e,cr}$ was determined from the estimated values of M_e (fig. 4), and P_e/P_0 is the product of the total-pressure ratios across the two oblique shocks. The value of P_e/P_0 was found to be greater than 0.985 for all cones and was therefore neglected in calculating the variation of P_4 with A_4.

The value of A_4 for which transition from supercritical to subcritical flow takes place was determined from M_e and A_e/A_3 in the manner described in reference 1.

The maximum theoretical total-pressure recovery for given values of $\theta_{c,1}$ and $\theta_{c,2}$ may be determined by finding the minimum Mach number $M_{3,min}$ at which the normal shock may occur and multiplying the total-pressure ratio across this normal shock by the total-pressure ratio across the two oblique shocks. The value of $M_{3,min}$ was found by determining the maximum theoretical internal contraction ratio A_e/A_3 allowable for the entrance Mach number M_e. The variation of the resulting maximum theoretical total-pressure recovery with $\theta_{c,2}$ for various values of $\theta_{c,1}$ was calculated for a free-stream Mach number M_0 of 1.85 and is plotted in figure 5(a).

Because the normal shock is assumed to occur at the throat, these curves are designated maximum supercritical total-pressure recoveries. The maximum theoretical subcritical total-pressure recoveries were also calculated for the same range of cone angles and are plotted in figure 5(b). These values are the product of the total-pressure ratios across the two oblique shocks and across a normal shock occurring at the inlet Mach number M_e. The best theoretical recovery with supercritical flow is obtained with a cone having an included angle of 30° at the tip and 50° beyond the break. For subcritical flow, the best theoretical cone is one with included angles of 40° at the tip and 64° beyond the break.

The preceding analysis is based on the assumption that a theoretically correct inlet is designed for each cone and tip projection. With the inlets actually used in this investigation, this condition was fulfilled only for part of the tests. The cases for which the bow wave remained ahead of the inlet correspond with the assumption only when the minimum area occurred at the inlet ($A_e/A_2 \leq 1.00$). For the remaining cases, the analysis is only a rough approximation.

PRESENTATION OF RESULTS

Schlieren observations. - Schlieren photographs of typical flow patterns obtained with the four cones are shown in figure 6. Figure 6(a) shows a type of flow often obtained when the tip projection was too small (contraction ratio too great). The configuration is the 20-40 cone with straight inlet. The area ratio A_4/A_1 is far in the supercritical region. Two distinct lines from the cone tip are visible, neither of which is inclined at the theoretical shock angle for a Mach number of 1.85 and cone half-angle of 10°. The inner line is inclined at an angle of 25° and the outer at an angle of 43°, whereas the theoretical shock angle is about 34°. Photographs of the same flow pattern with exposures of the order of microseconds show that the inner line is a boundary between two distinct flow regions. The region nearest the cone surface is apparently subsonic, inasmuch as no shock occurs at the break in the cone. The oblique shock angle (43°) is approximately correct for a cone angle equal to that defined by the limit of the observed subsonic flow region ($\theta_c = 25°$).

With the 20-40 cone at optimum tip projection, three oblique shocks appeared ahead of the inlet (fig. 6(b)). The second arises somewhat ahead of the break in the cone surface and the third somewhat

beyond the break. A similar succession of three oblique shocks was observed with each of the cones tested. The second and third shocks are attributed to a bridging of the break by the boundary layer. The second shock presumably arises where the boundary layer begins to thicken and the third shock where the boundary-layer bridge terminates.

The oblique shocks pass outside the entrance lip and the bow wave curves toward the interior (fig. 6(c)) with the 30-50 cone at optimum tip projection. The second and third oblique shocks arising near the break in the cone surface seem to be of almost equal intensity.

The inlet flow corresponding to the highest total-pressure recovery attained during the investigation is shown in figure 6(d). Three oblique shocks again appear ahead of the inlet. The normal shock stands ahead of the entrance and the flow spills over around the entrance lip.

The flow pattern corresponding to the highest total-pressure recovery obtained with the straight inlet is shown in figure 6(e). The normal shock again stands well ahead of the inlet, extending almost to the origin of the third oblique shock.

With the 40-70 cone at a tip projection somewhat greater than optimum, the normal shock again stands ahead of the inlet almost to the origin of the third oblique shock (fig. 6(f)). In figure 6(g) the outlet area has been decreased somewhat. The normal shock has disappeared and subsonic flow prevails behind the third oblique shock. That this flow pattern is highly unstable is shown by figure 6(h), which is an exposure of the order of microseconds for the same experimental conditions. The bow wave is out almost to the cone tip and considerable turbulence is visible in the flow behind it. A faint image of this shock pattern was also visible in the original of figure 6(g), which is a 1/50-second exposure.

Variation of total-pressure recovery with outlet area. - The variation of total-pressure recovery P_4/P_0 with outlet-inlet area ratio A_4/A_1 is shown in figure 7. The theoretical curves for each cone-inlet combination were calculated by methods previously discussed. In the supercritical region these theoretical curves should lie to the left of the data because the build-up of the boundary layer at the outlet tends to reduce the actual flow area below the measured geometrical area. An examination of figure 7 indicates many exceptions to this prediction. These exceptions occurred when the inlet flow was subsonic throughout the test. Under this condition

the inlet flow spills around the entrance lip, and consequently $(\rho V)_e/(\rho V)_{e,cr}$ is less than the theoretically predicted value. For the 20-40 cone the inlet flow was subsonic for all values of A_4/A_i only when the straight inlet was used with tip projections of 1.50 and 1.75 inches. (See fig. 7(a).) The inlet flow was subsonic because, for these tip projections, the internal contraction ratio was too great to allow entry of the normal shock. With the other cones, however, data fell to the left of the theoretical curves for the maximum as well as for some of the minimum tip projections, which indicates that M_e became subsonic for large tip projections. Although the theoretically estimated values of M_e were subsonic only for the 40-70 cone (fig. 4), these estimated values neglect boundary-layer effects and would consequently be expected to be greater than actual values.

The tip projections for which M_e was subsonic for the 30-50, 30-60, and 40-70 cones may be determined from figures 7(c) to 7(h). For the 30-50 cone, the data fall to the left of the theoretical curve for the maximum tip projection (1.875 in.) with both inlets and also for the minimum tip projection with the straight inlet. For the 30-60 cone, the data fall to the left for all tip projections with the straight inlet and for the maximum tip projection with the curved inlet. For the 40-70 cone the data fall to the left for all tests except those at the smallest tip projections with the curved inlet. An examination of schlieren photographs taken during the investigation confirmed the expectation that the flow spilled over for all outlet areas when the data fell very close to or to the left of the theoretical curves in the supercritical region. Comparison of figure 7 with similar results in reference 1 (fig. 6) shows that in the vicinity of optimum A_4/A_i the total-pressure recovery was more sensitive to changes in outlet area for double-shock than for single-shock cones and that the total-pressure recoveries in the subcritical region are lower than those obtained with single-shock cones.

Effect of angle of attack. - Several of the tests with the 30-60 cone, which yielded the highest pressure recoveries, were repeated at an angle of attack of 5°. The results are compared with those obtained at an angle of attack of 0° (fig. 8). With the configuration giving the highest total-pressure recovery obtained (fig. 8(b), curved inlet, L = 1.56 in.), the maximum total-pressure recovery dropped from 94.5 percent at 0° angle of attack to 89.9 percent at 5° angle of attack. Figure 8(a) presents the results for the same configuration at slightly smaller tip projection. The maximum recovery dropped from 94.3 to 89.3 percent. With the straight inlet

at optimum tip projection (fig. 8(c)), the recovery dropped from 94.3 to 90.2 percent. At a slightly greater tip projection (fig. 8(d)), the recovery dropped from 93.7 to 89.3 percent. These results indicate that the effect of angle of attack is slightly greater for the curved than for the straight inlet. Comparison with the results obtained with single-shock cones indicates that the effect of angle of attack is somewhat greater for double-shock cones. With single-shock cones, the total-pressure recovery dropped from 92.2 to 90.8 percent for the configuration giving the highest total-pressure recovery (reference 1).

Pressure and Mach-number distribution at diffuser outlet. - Static- and total-pressure distributions at an angle of attack of 0° for the configuration giving the highest total-pressure recovery are presented in figures 9(a) and 9(b). The corresponding distributions at an angle of attack of 5° are included in figures 9(c) and 9(d). The location of the tubes in the rake is shown. The position of the pitot-static rake with which these distributions were measured is shown in figure 1(a). The data points correspond to the tube locations shown in these sketches. Because the static-pressure distribution is fairly uniform for both 0° and 5° angles of attack, the total-pressure distributions give an indication of the uniformity of the velocity at the diffuser outlet. Except for values of A_4/A_i far in the supercritical region, these velocity distributions seem satisfactory, although at 5° angle of attack the asymmetry of the entrance flow is apparently carried through to the diffuser outlet. This asymmetry of the flow at an angle of attack of 5° can be seen more clearly in figure 10, where the Mach-number distribution (calculated from the pressure distributions of fig. 9) for the highest total-pressure recovery is plotted for angles of attack of 0° and 5°. The effect of an increase in angle of attack is seen to be much more disturbing than any wake effects due to the cone-support body.

Effect of tip projection on maximum total-pressure recovery. - The maximum total-pressure recoveries of figure 7 are replotted as functions of tip projection and internal contraction ratio in figure 11. The variation with tip projection is similar to that obtained with single-shock cones (reference 1). At small tip projections, for which the oblique shocks do not pass outside the entrance lip (fig. 2), the recovery is relatively low. As explained in reference 1, the normal shock could not pass into the diffuser for such tip projections. (With the straight inlet, the contraction ratio was greater than that required to reduce M_0 to unity and choking occurred at A_3, whereas with the curved inlet the angle of the entrance lip caused detachment of the shock unless the flow was first deflected through an external

oblique shock.) As the tip projection was increased, an optimum value was reached beyond which the recovery again dropped. From figure 11(c) the range of tip projections for which the recovery remained fairly close to the maximum value may be estimated to be about one-eighth inch. The tip projections were varied in steps of one-eighth inch, except near the optimum points of some of the curves where the sequence was reduced to one-sixteenth inch because it seemed possible that a higher total-pressure recovery might be obtained.

The highest total-pressure recoveries were obtained with the 30-60 cone (fig. 11(c)). With the curved inlet the maximum outlet total pressure was 94.5 percent of the free-stream value; with the straight inlet, 94.3 percent. These recoveries correspond to efficiencies of kinetic-energy conversion (as defined in reference 3) of 97.6 and 97.5 percent, respectively. All of the cones except the 20-40 cone yielded maximum total-pressure recoveries greater than 92 percent (efficiencies greater than 96.5 percent).

ANALYSIS OF RESULTS

The theoretical maximum recoveries of figure 5 are compared with those actually obtained (fig. 11) in the following table:

Cone (deg)	Theoretical maximum P_4/P_0		Experimental maximum P_4/P_0	
	Supercritical flow	Subcritical flow	Straight inlet	Curved inlet
20-40	0.980	0.943	0.909 (super)	0.894 (super)
30-50	.991	.968	.937 (sub)	.929 (super)
30-60	.986	.973	.943 (sub)	.945 (sub)
40-70	.983	.981	.922 (sub)	.940 (sub)

The notes (super) and (sub) after each of the experimental values indicate that the value was attained with supercritical or subcritical flow, respectively, as determined from schlieren observations. The minimum difference between theoretical and experimental maximum recoveries, which gives an indication of the losses in the subsonic portion of the diffuser, is about 3.0 percent (30-60 cone). Probably the additional oblique shock caused by boundary-layer separation was beneficial in attaining these high recoveries. This additional shock

may also account for the discrepancy between the theoretical and the actual variation of maximum total-pressure recovery with cone angles.

The preceding table shows that the maximum recovery was obtained with the straight inlet for the 20-40 and the 30-50 cones and with the curved inlet for the 30-60 and the 40-70 cones. For the 20-40 and the 30-50 cones, the flow expands from the entrance to the interior with the curved inlet ($A_e/A_3 < 1.0$, see fig. 4). With such expansion, the normal shock occurs in the interior at a Mach number greater than the entrance Mach number M_e, which probably accounts for the relatively low performance of the first two cones with the curved inlet. For the other two cones (30-60 and 40-70) the inlet flow was subsonic for both the curved and the straight inlets and hence the expansion obtained with the curved inlet was harmless. The more nearly parallel entrance flow probably accounts for the higher total-pressure recovery obtained with the curved inlet for these two cones.

In reference 1 the condition determining optimum experimental tip projection for the curved inlet was that the oblique shock must pass outside the entrance lip, whereas, for the straight inlet, optimum tip projection occurred when the internal contraction ratio was approximately equal to the theoretical maximum for the entrance Mach number M_e.

Similar conditions may be established for the double-shock cones. In the following table, the third column presents the optimum theoretical internal contraction ratios A_e/A_3 (determined for $M_e = \frac{1}{2}(M_{2,c} + M_{2,b})$; the fourth column presents the tip projections corresponding to these theoretical optimum internal contractions; the fifth column gives the minimum tip projection for external oblique shocks (determined from schlieren photographs); and the last column gives the experimental optimum tip projections of figure 11:

Cone (deg)	Inlet	Theoretical optimum A_e/A_3	Tip projection for theoretical optimum A_e/A_3 (in.)	Minimum tip projection for external oblique shocks (in.)	Experimental optimum tip projection (in.)
20-40	Straight	1.085	2.08	2.00	2.125
30-50	---do---	1.055	1.64	1.625	1.750
30-60	---do---	1.040	1.52	1.50	1.6875
40-70	---do---	1.000	1.31	1.375	1.500
20-40	Curved	1.085	1.52	1.75	1.875
30-50	---do---	1.055	1.20	1.50	1.625
30-60	---do---	1.040	1.18	1.50	1.5625
40-70	---do---	1.000	1.03	1.25	1.375

A comparison of the last two columns shows that the optimum tip projection in each case is about one-eighth inch greater than the minimum tip projection for which the oblique shocks pass outside the diffuser entrance lip. The contraction-ratio condition that determined the optimum tip projection for the straight inlet in reference 1 is not applicable for either inlet with the double-shock cones. For the first three cones, with straight inlet, the oblique shocks pass outside at about the same tip projection for which maximum theoretical contraction ratio occurs. The two conditions are therefore indistinguishable for these combinations. For the remaining cone-inlet combinations, the value of A_e/A_3 is below the theoretical maximum before the oblique shocks pass outside; hence only the oblique-shock condition is applicable.

The requirement that the oblique shocks pass outside the entrance lip for optimum total-pressure recovery may be explained as follows: With the straight inlet, the total contraction ratio A_0/A_3 is greater than that required to lower the free-stream Mach number ($M_0 = 1.85$) to unity unless the flow is first contracted through external oblique shocks. Thus, if the entrance Mach number is supersonic ($M_e > 1.0$), the flow is choked at the minimum area A_3 and the normal shock cannot enter the diffuser. If M_e is subsonic, the flow will be accelerated to sonic velocity at A_3 and a normal shock will occur at some position after the throat. In either case the normal shock occurs at a Mach number higher than optimum and a lower total-pressure recovery results.

With the curved inlet, the angle of the entrance lip was sufficient to cause a bow wave to form ahead of the diffuser inlet unless the free-stream flow was first deflected through external oblique shocks. If M_e is already subsonic, as with the 40-70 cone, then the bow wave is, of course, limited to the supersonic region and the reason for lower recoveries with L less than optimum is not obvious. If M_e is supersonic, however, the bow wave extends to the cone surface for tip projections less than the minimum value for which the oblique shocks pass outside the entrance lip. As the tip projection is increased, M_e decreases (fig. 4) and the total-pressure loss across the bow wave should decrease.

As the tip projection L was increased beyond the optimum value, the cylindrical portion of the cone body appeared ahead of the diffuser inlet, and schlieren photographs (for example, fig. 6(f)) showed evidence of flow separation as the stream turned toward the direction of the diffuser axis. This separation may account for the decrease in total-pressure recovery for values of L greater than optimum.

SUMMARY OF RESULTS

The total-pressure recovery of a shock diffuser with projecting double-shock cones was investigated. A series of four cones was used. Each cone was tested with a straight and with a curved inlet and the optimum tip projection was found for each configuration. The results were compared with those obtained with single-shock cones. The results are as follows:

1. The maximum total-pressure recovery was somewhat higher than that attained with single-shock cones. A value of 94.5 percent of the free-stream total pressure was recovered, as compared with the maximum recovery of 92.2 percent attained with single-shock cones. (In terms of the efficiency of kinetic-energy conversion, these maximum values correspond to 97.6 percent for the double-shock cones and 96.5 percent for the single-shock cones.) This maximum total-pressure recovery was obtained with the curved inlet in combination with a cone having an included angle of 30° ahead of and 60° behind the break in the cone surface. Several configurations gave maximum total-pressure recoveries greater than 92.0 percent at an angle of attack of 0°.

2. The effect of angle of attack on the maximum recovery was somewhat greater for the double-shock than for the single-shock cones. The maximum value of 94.5 percent at 0° angle of attack was reduced to 89.9 percent at 5° angle of attack.

3. The maximum recoveries were obtained with subsonic inlet flow. For outlet areas less than optimum the total-pressure recovery dropped to lower values than those obtained with single-shock cones.

4. With each cone, three oblique shocks appeared ahead of the diffuser inlet instead of the two theoretically predicted. The additional shock resulted from a bridging of the break in the cone surface by the boundary layer.

5. The effect of the cone-support body on the velocity distribution at the diffuser outlet for the best configuration was found to be negligible in comparison with the effect of angle of attack.

Flight Propulsion Research Laboratory,
National Advisory Committee for Aeronautics,
Cleveland, Ohio, June 10, 1947.

REFERENCES

1. Moeckel, W. E., Connors, J. F., and Schroeder, A. H.: Investigation of Shock Diffusers at Mach Number 1.85. I - Projecting Single-Shock Cones. NACA RM No. E6K27, 1946.

2. Ferri, Antonio: Application of the Method of Characteristics to Supersonic Rotational Flow. NACA TN No. 1135, 1946.

3. Kantrowitz, Arthur, and Donaldson, Coleman duP.: Preliminary Investigation of Supersonic Diffusers. NACA ACR No. L5D20, 1945.

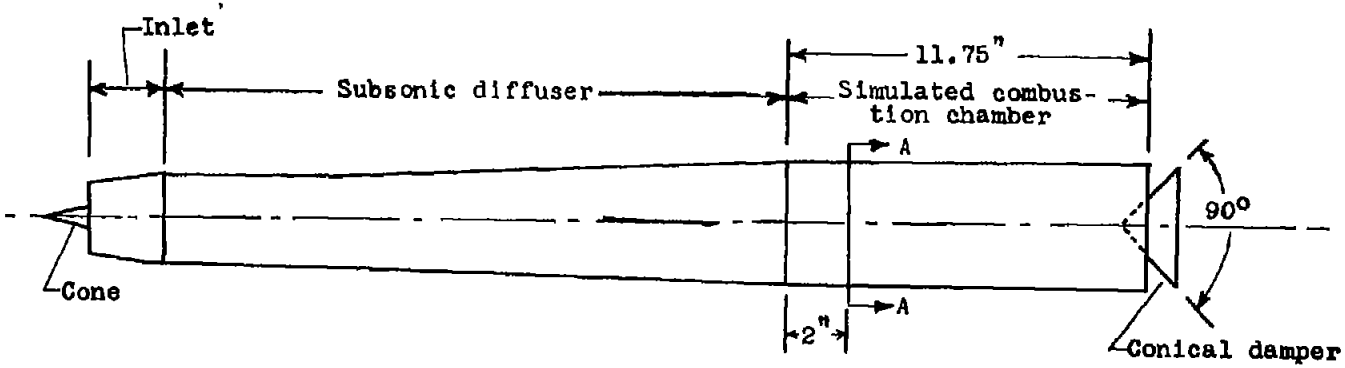

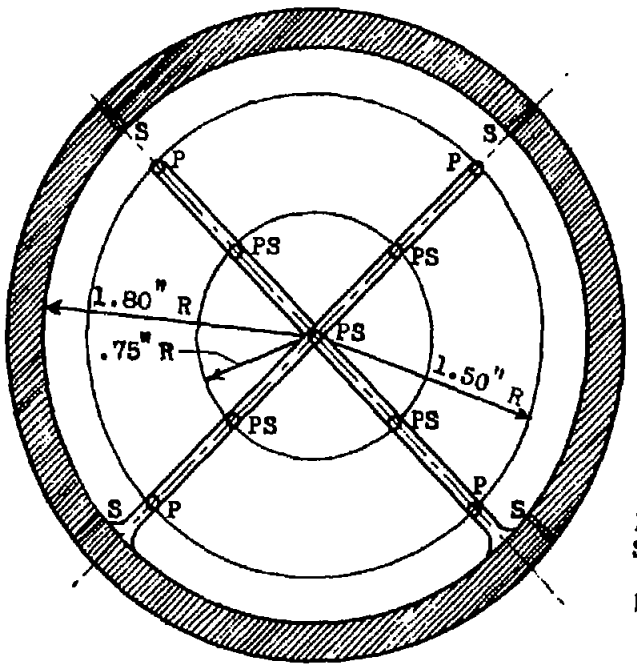

NATIONAL ADVISORY
COMMITTEE FOR AERONAUTICS

P Pitot tube
S Static-pressure orifice
PS Pitot-static tube

Section A-A

(a) Diffuser and simulated combustion chamber with pressure instrumentation.

Figure 1.- Experimental model.

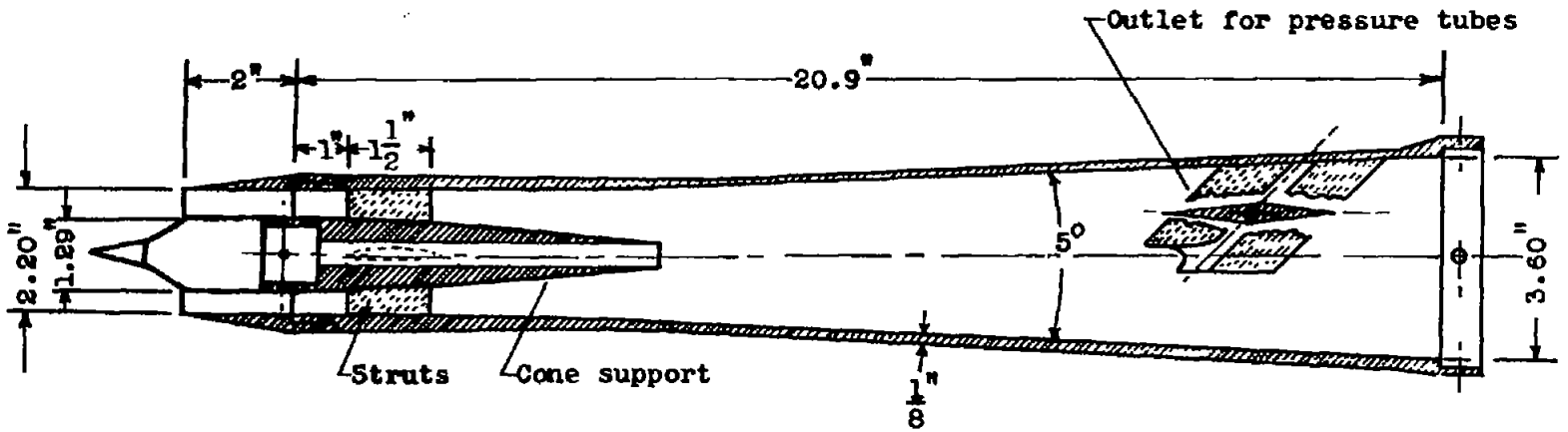

(b) Diffuser body and cone support.

NATIONAL ADVISORY
COMMITTEE FOR AERONAUTICS

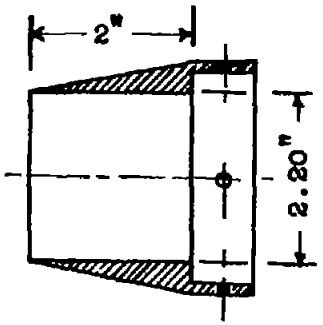

(c) Straight inlet.

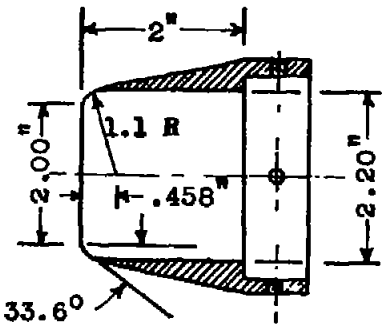

(d) Curved inlet.

Figure 1.- Concluded. Experimental model.

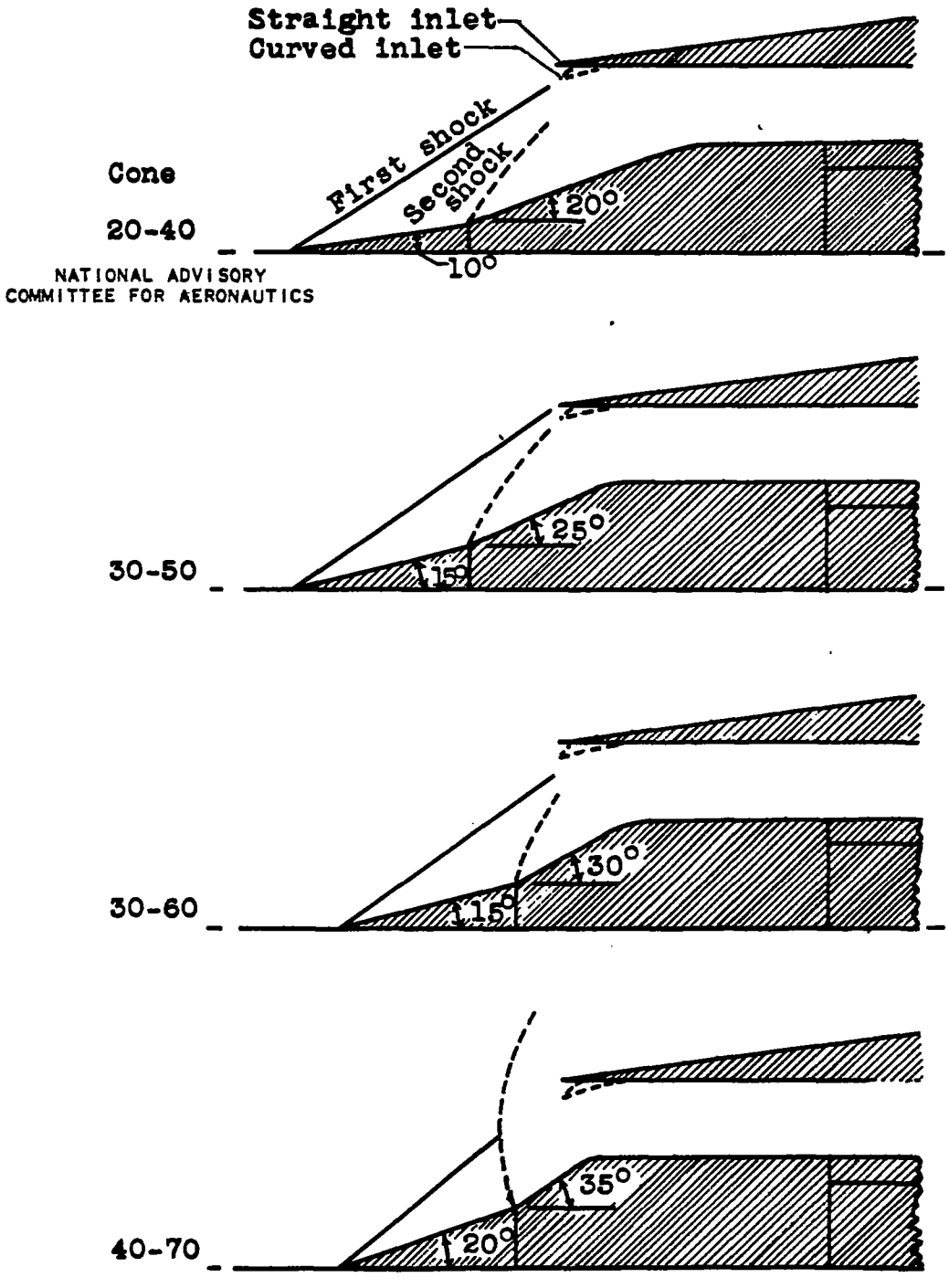

Figure 2.- Sketches of cones showing theoretical locations of oblique shocks for minimum tip projections. (Bow wave at inlet not shown.)

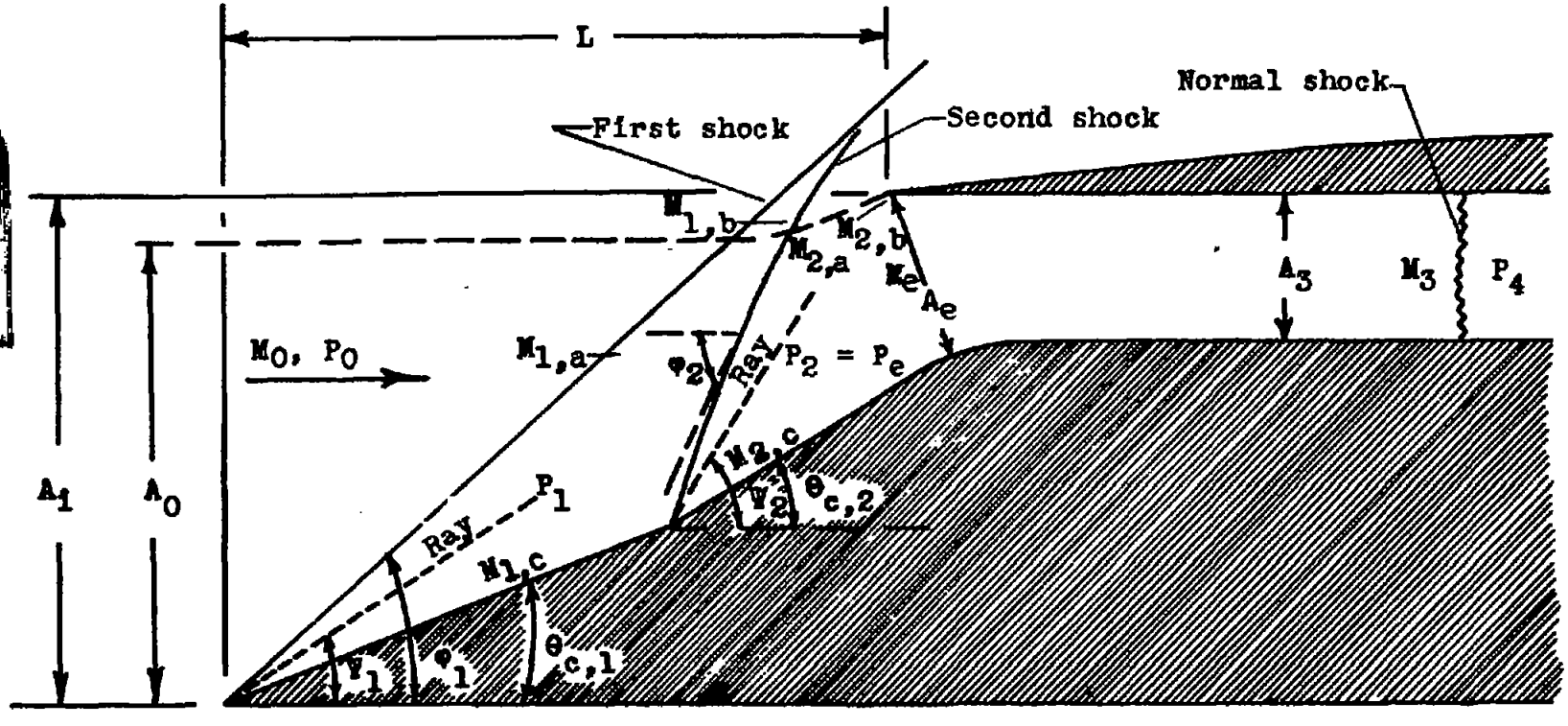

Figure 3.- Notation used at shock-diffuser inlet.

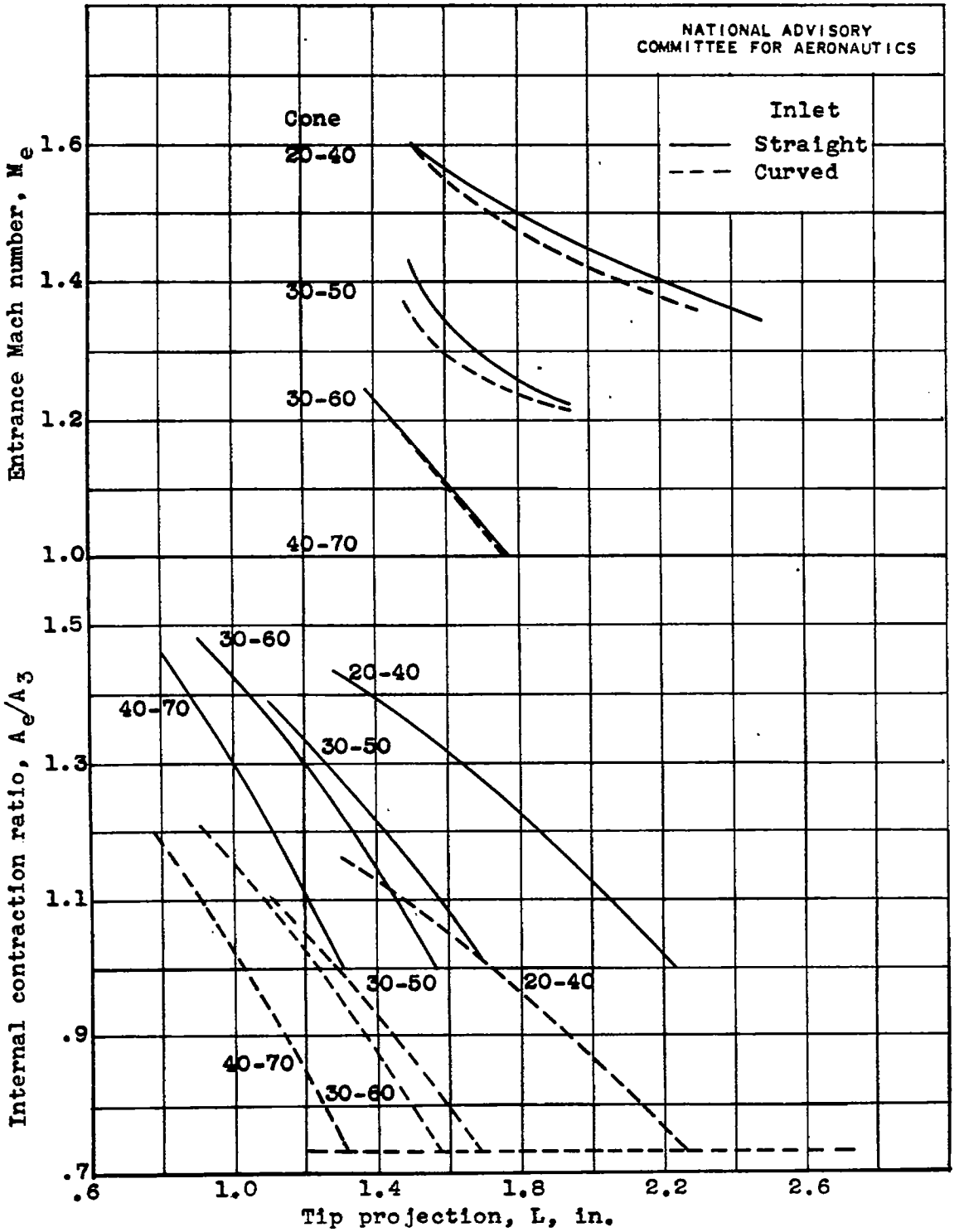

Figure 4.- Variation of estimated average entrance Mach number and internal contraction ratio with tip projection for cones shown in figure 2.

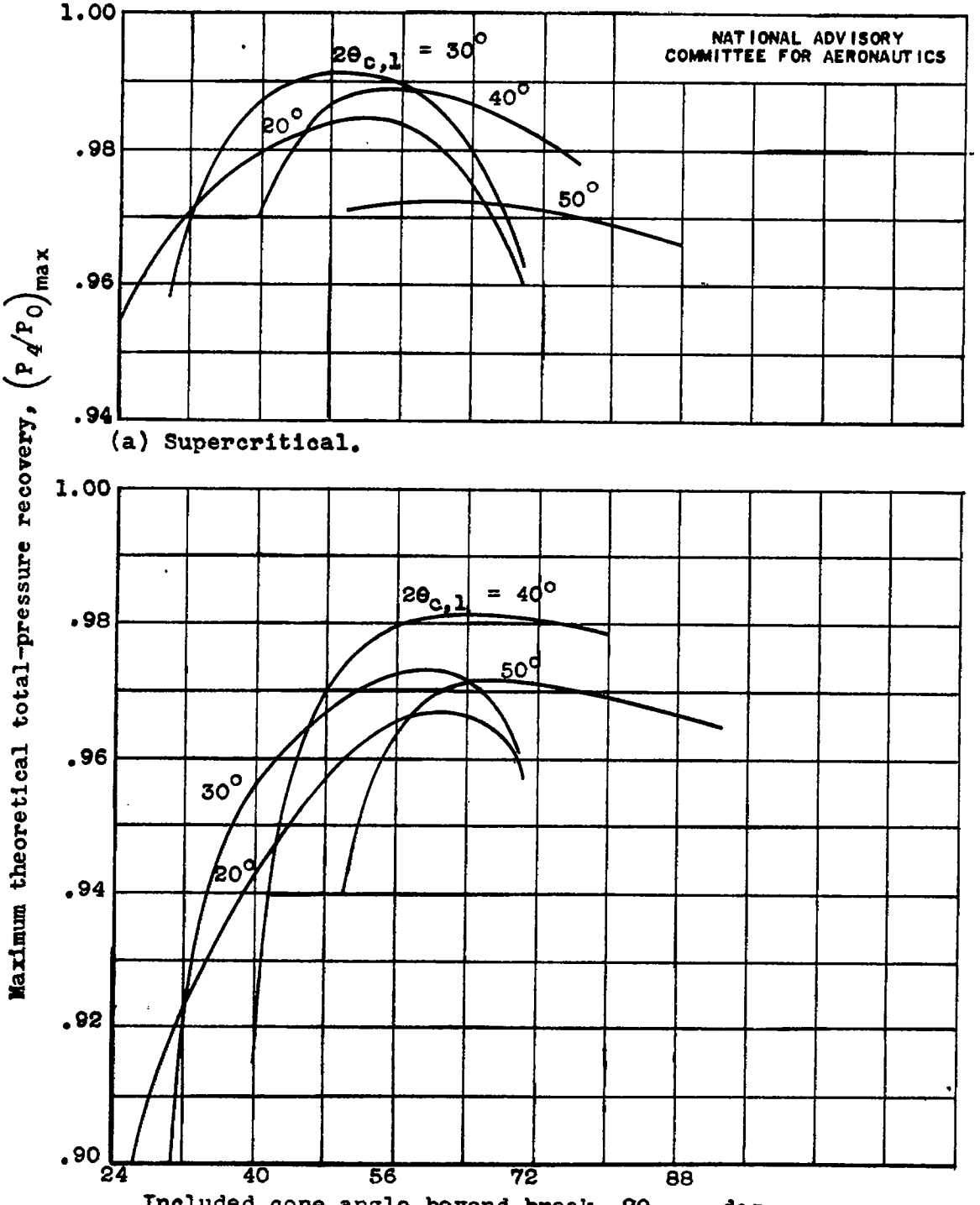

Figure 5.- Theoretical maximum total-pressure recovery with two oblique shocks ahead of diffuser inlet.

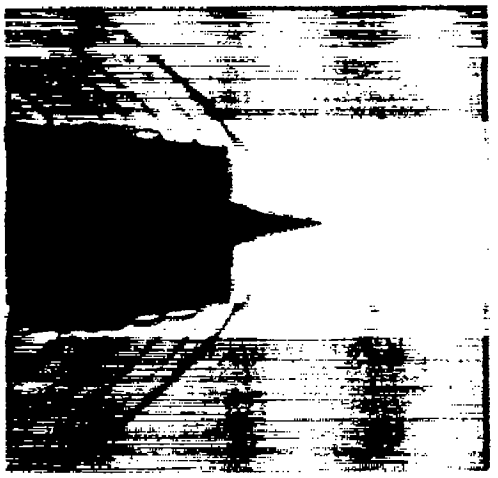

(a) Supercritical flow with tip projections less than optimum: 20-40 cone; straight inlet; L, 1.50 inches; A_4/A_i, 1.911; P_4/P_0, 0.372.

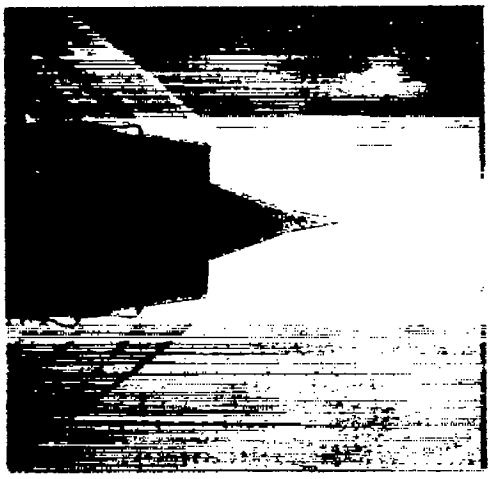

(b) Flow pattern with optimum tip projection: 20-40 cone; straight inlet; L, 2.125 inches; A_4/A_i, 0.780; P_4/P_0, 0.874.

(c) Flow pattern with optimum tip projection: 30-50 cone; curved inlet; L, 1.625 inches; A_4/A_i, 0.806; P_4/P_0, 0.865.

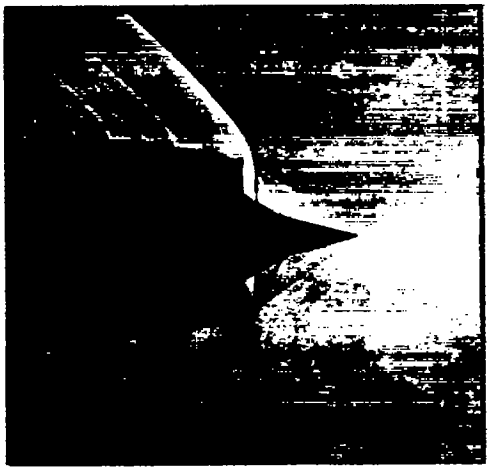

NACA
C-17245
11-26-46

(d) Flow pattern corresponding to highest total-pressure recovery attained: 30-60 cone; curved inlet; L, 1.5625 inches; A_4/A_i, 0.615; P_4/P_0, 0.945.

Figure 6. - Schlieren photographs of typical flow patterns with cones of figure 2 at angle of attack of 0°.

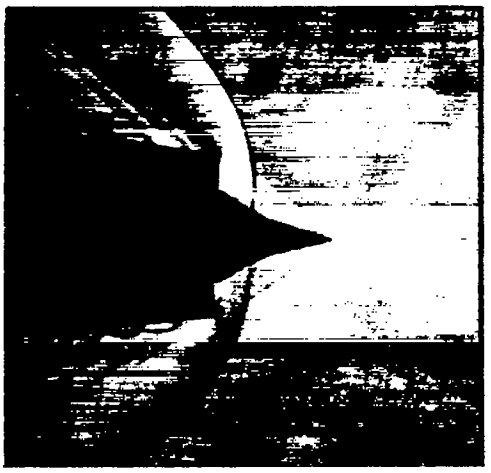

(e) Flow pattern for highest total-pressure recovery attained with straight inlet: 30-60 cone; L, 1.6875 inches; A_4/A_i, 0.567; P_4/P_0, 0.943.

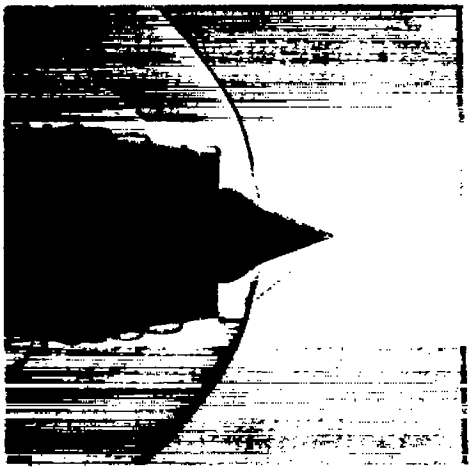

(f) Subcritical flow with high total-pressure recovery: 40-70 cone; straight inlet; L, 1.625 inches; A_4/A_i, 0.427; P_4/P_0, 0.912.

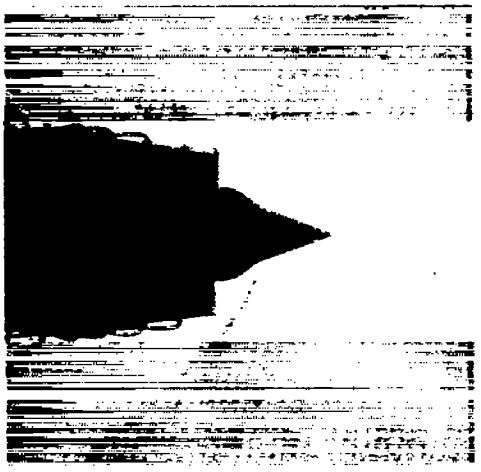

(g) Unstable subcritical flow pattern with 1/50-second exposure: 40-70 cone; straight inlet; L, 1.625 inches; A_4/A_i, 0.333; P_4/P_0, 0.817.

NACA
C-17246
11-26-46

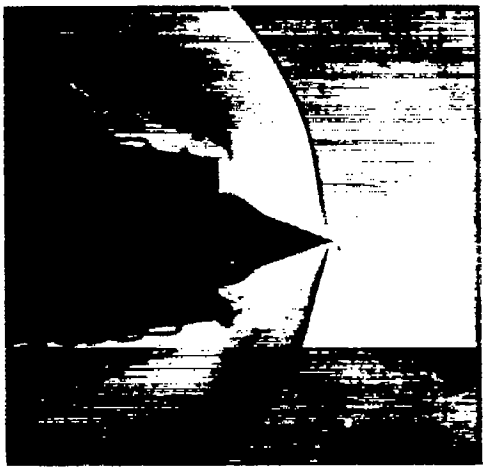

(h) Unstable subcritical flow pattern with microsecond exposure: 40-70 cone; straight inlet; L, 1.625 inches; A_4/A_i, 0.333; P_4/P_0, 0.817.

Figure 6. - Concluded. Schlieren photographs of typical flow patterns with cones of figure 2 at angle of attack of 0°.

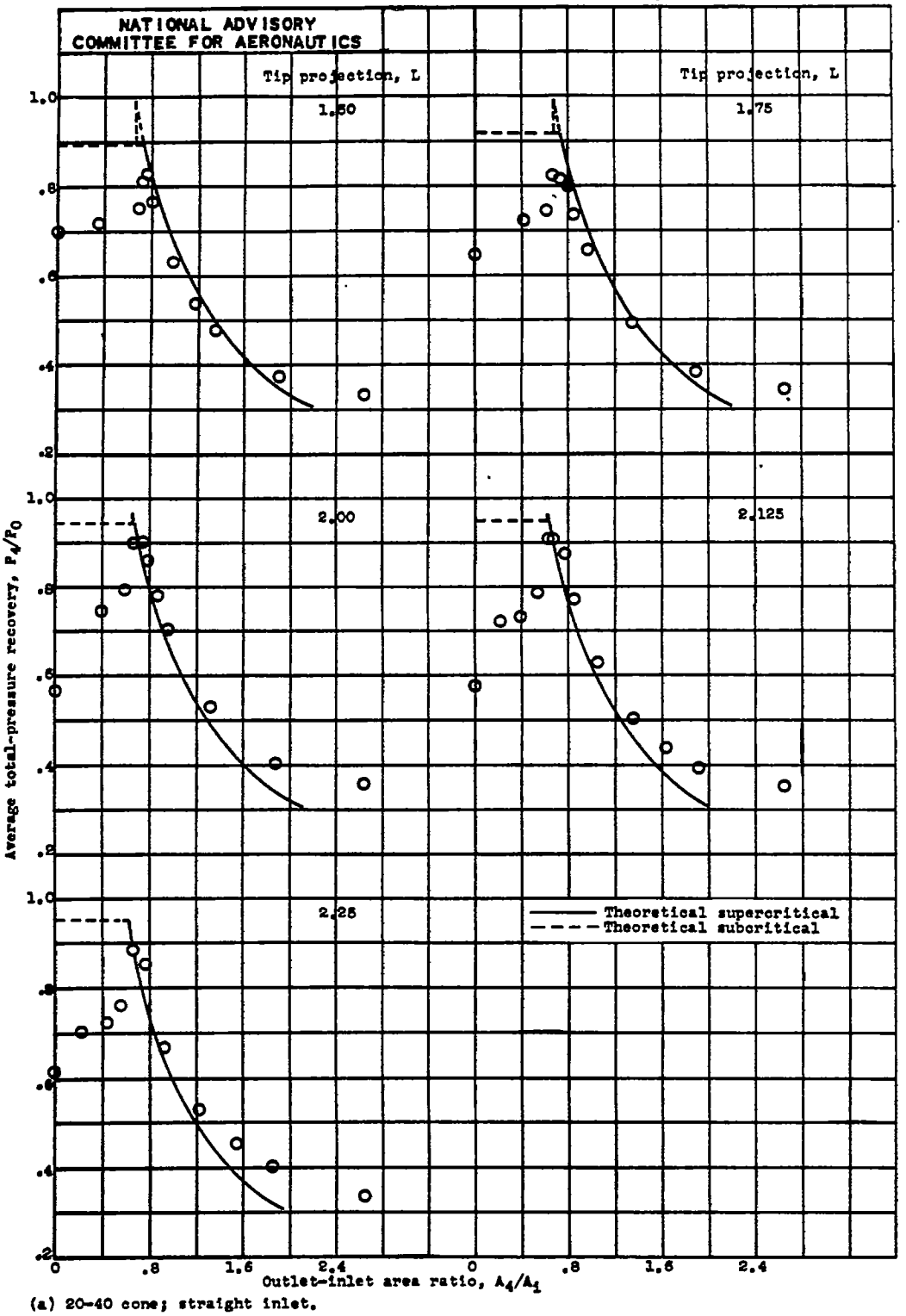

(a) 20-40 cone; straight inlet.

Figure 7.- Variation of total-pressure recovery with outlet-inlet area ratio at angle of attack of 0°.

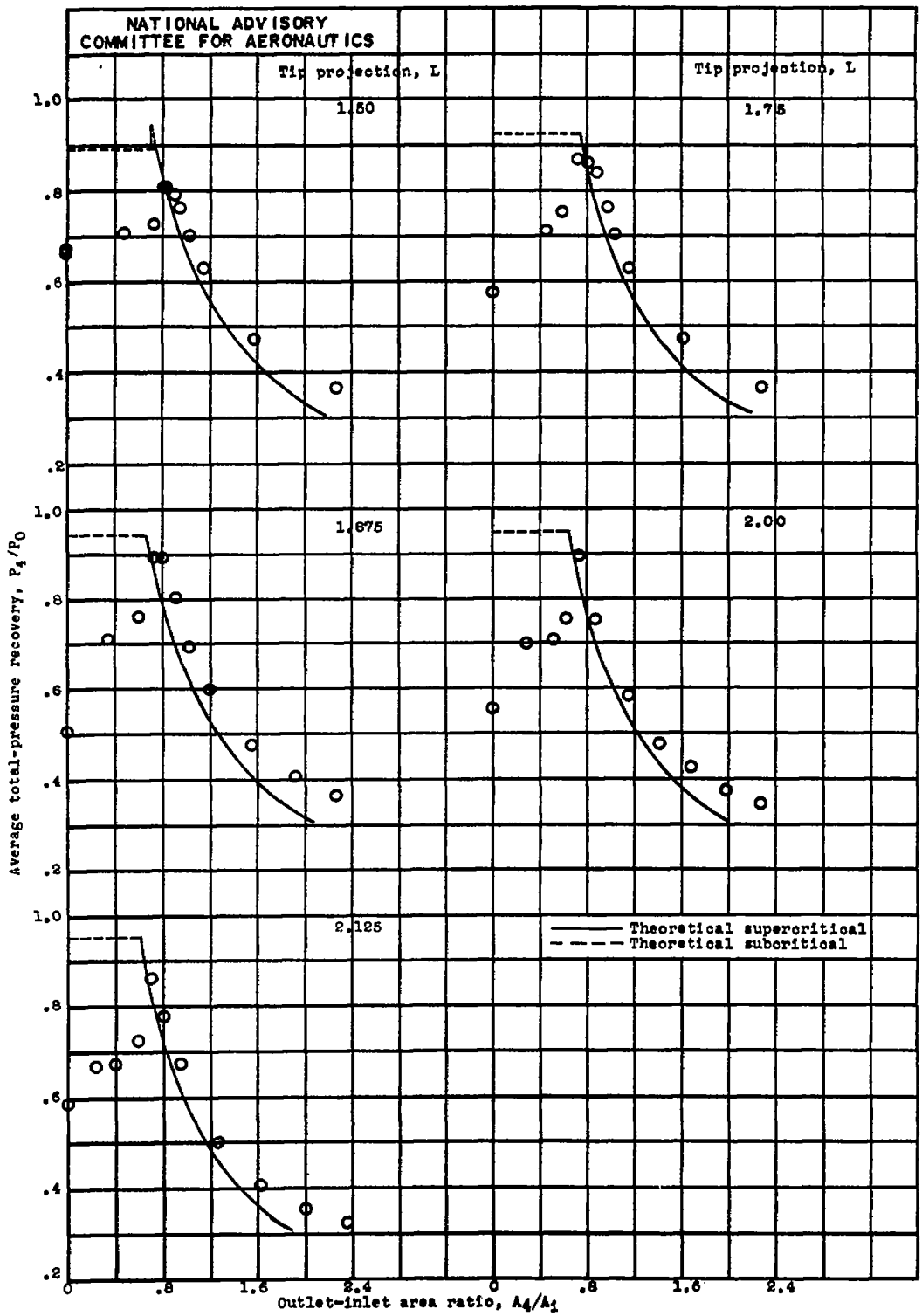

(b) 20-40 cone; curved inlet.

Figure 7.- Continued. Variation of total-pressure recovery with outlet-inlet area ratio at angle of attack of 0°.

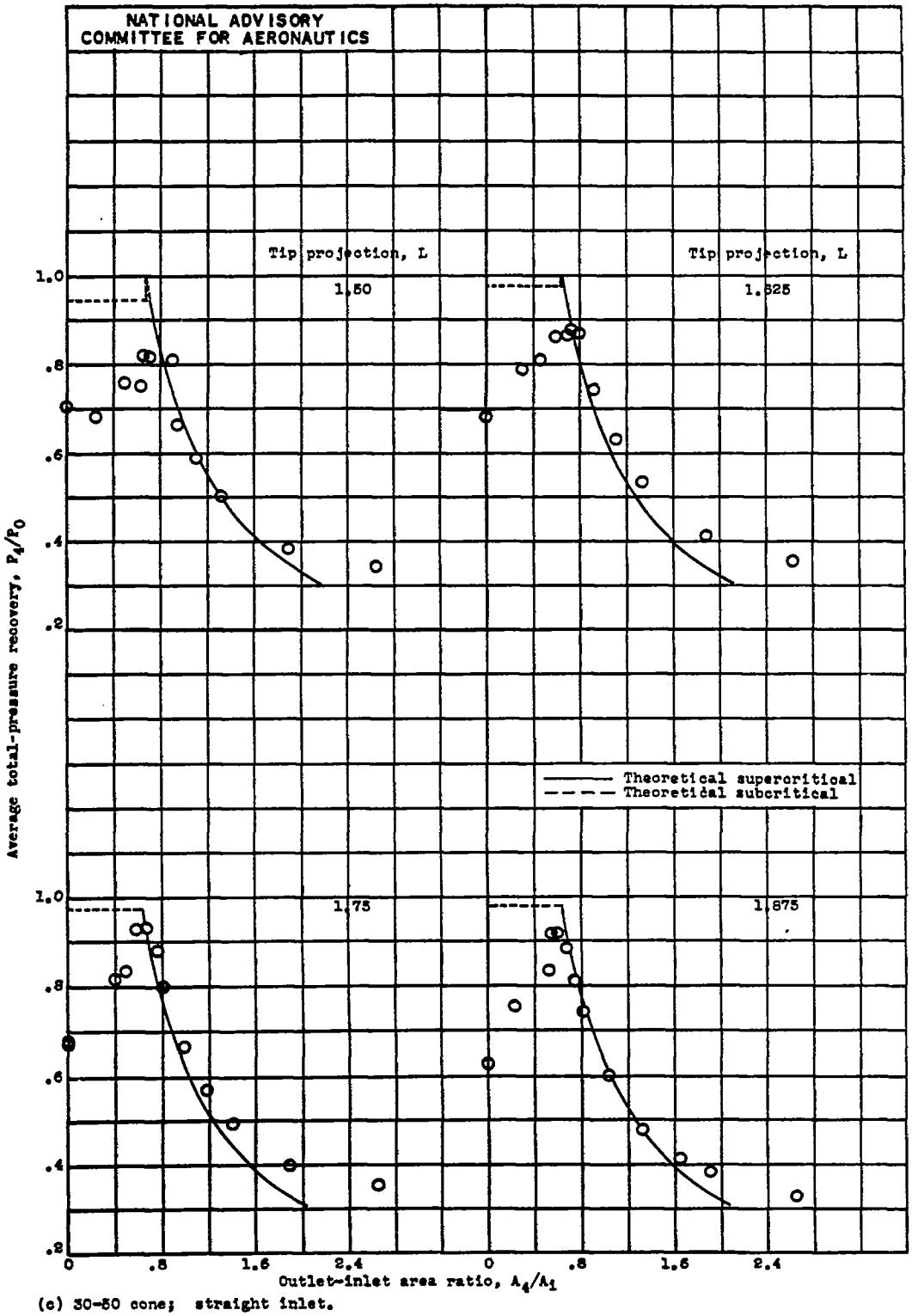

(c) 30-50 cone; straight inlet.

Figure 7.- Continued. Variation of total-pressure recovery with outlet-inlet area ratio at angle of attack of 0°.

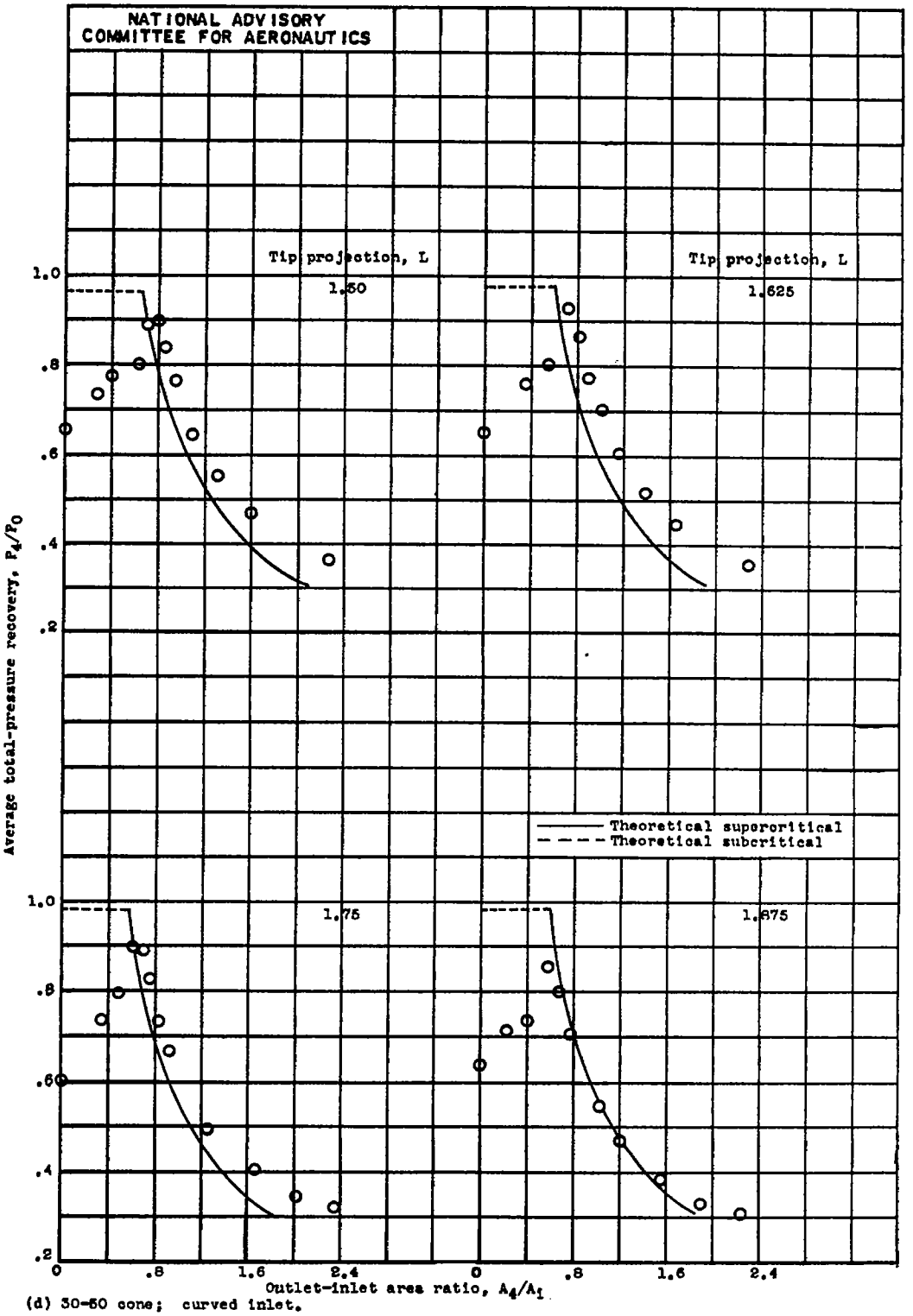

(d) 30-60 cone; curved inlet.

Figure 7.- Continued. Variation of total-pressure recovery with outlet-inlet area ratio at angle of attack of 0°.

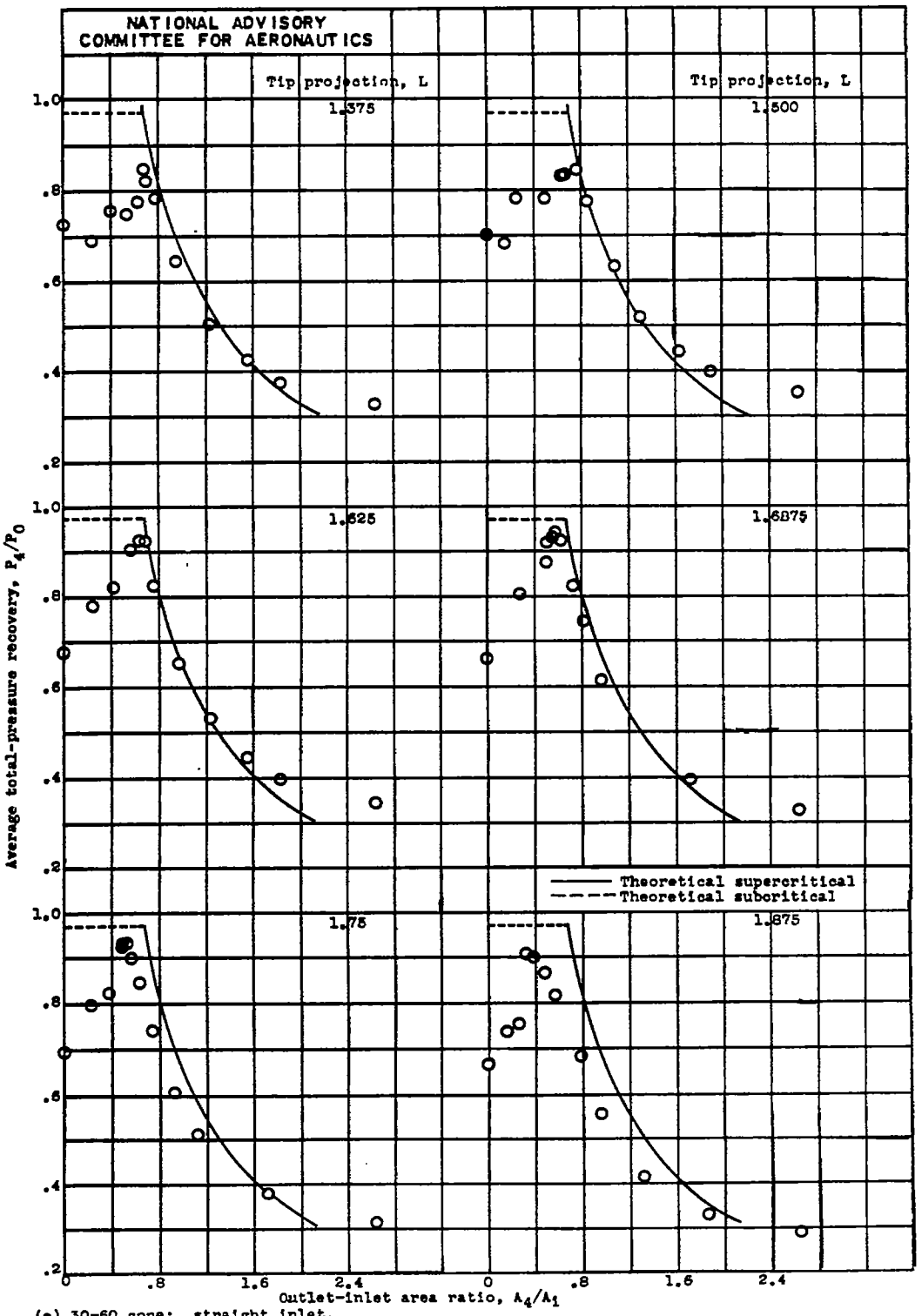

(e) 30-60 cone; straight inlet.

Figure 7.- Continued. Variation of total-pressure recovery with outlet-inlet area ratio at angle of attack of 0°.

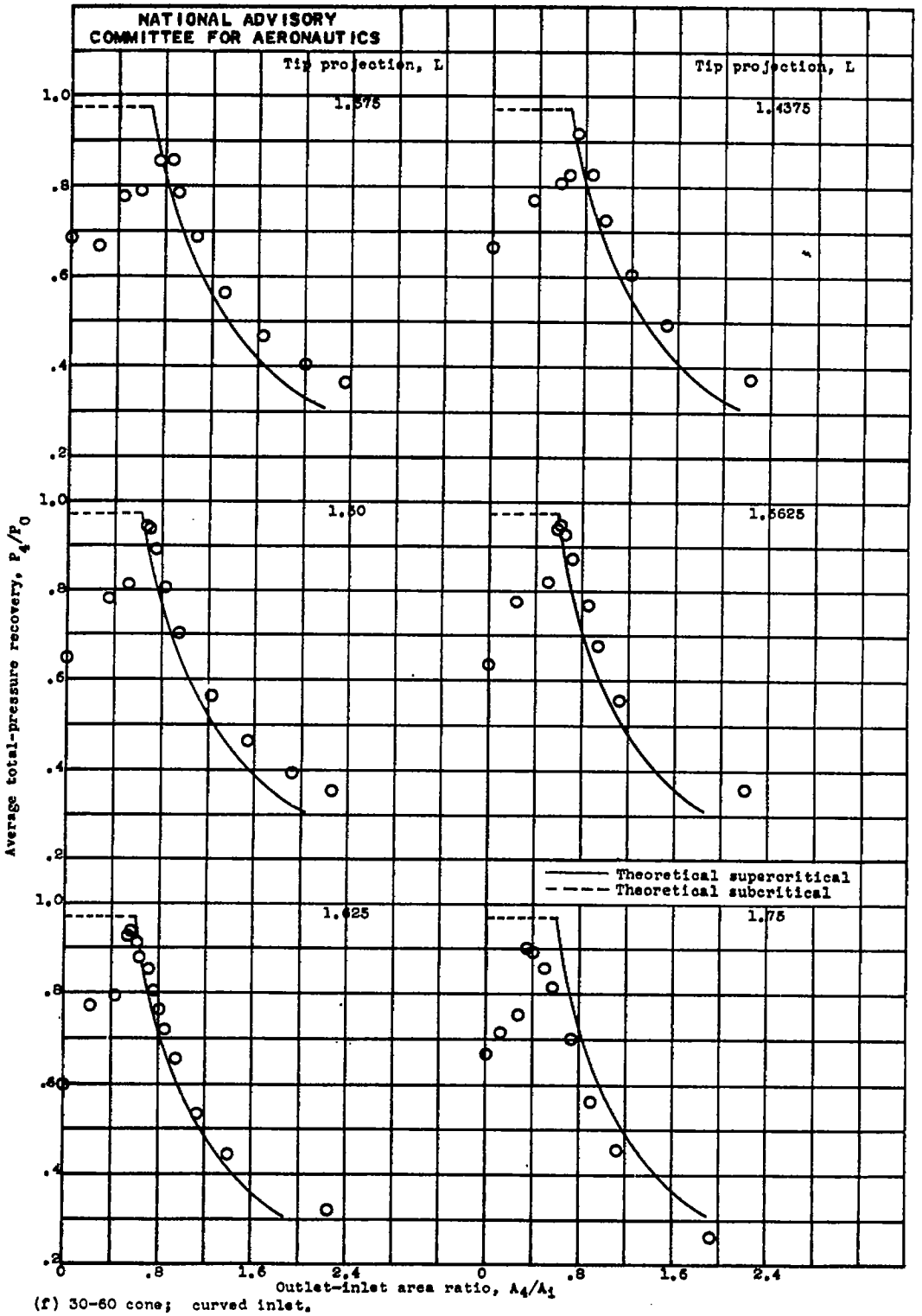

(f) 30-60 cone; curved inlet.

Figure 7.- Continued. Variation of total-pressure recovery with outlet-inlet area ratio at angle of attack of 0°.

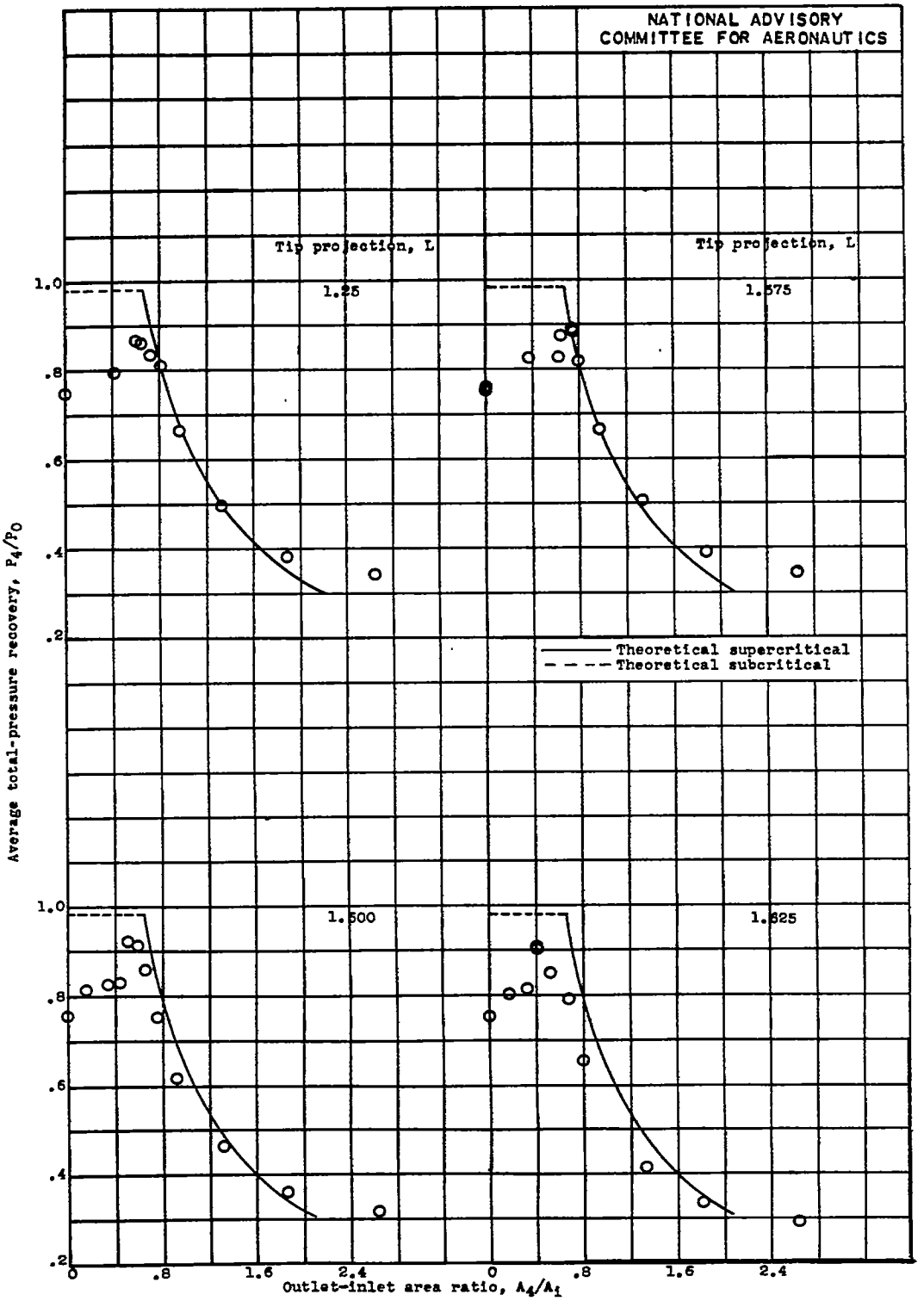

(g) 40-70 cone; straight inlet.

Figure 7.- Continued. Variation of total-pressure recovery with outlet-inlet area ratio at angle of attack of 0°.

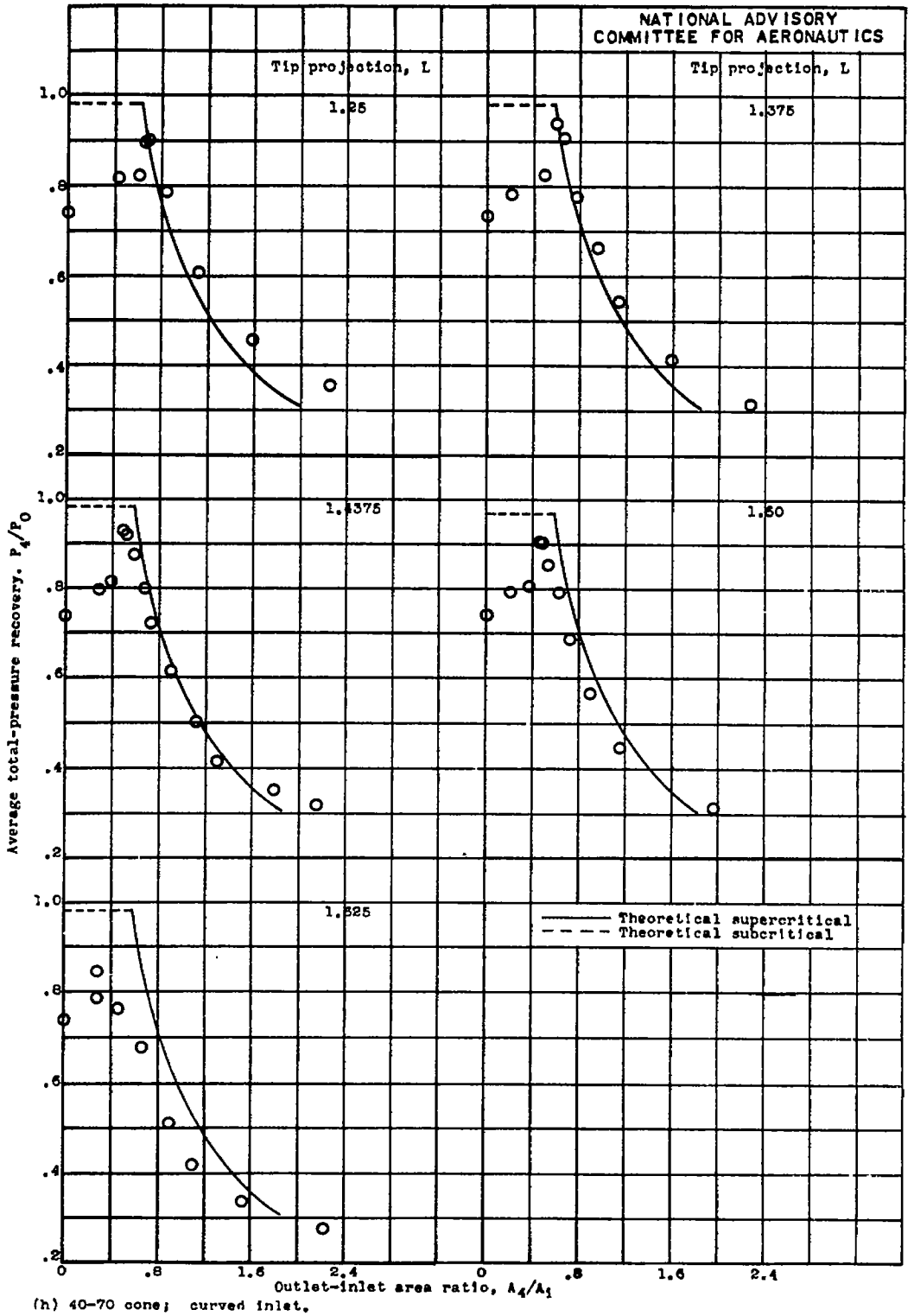

(h) 40-70 cone; curved inlet.

Figure 7.- Concluded. Variation of total-pressure recovery with outlet-inlet area ratio at angle of attack of 0°.

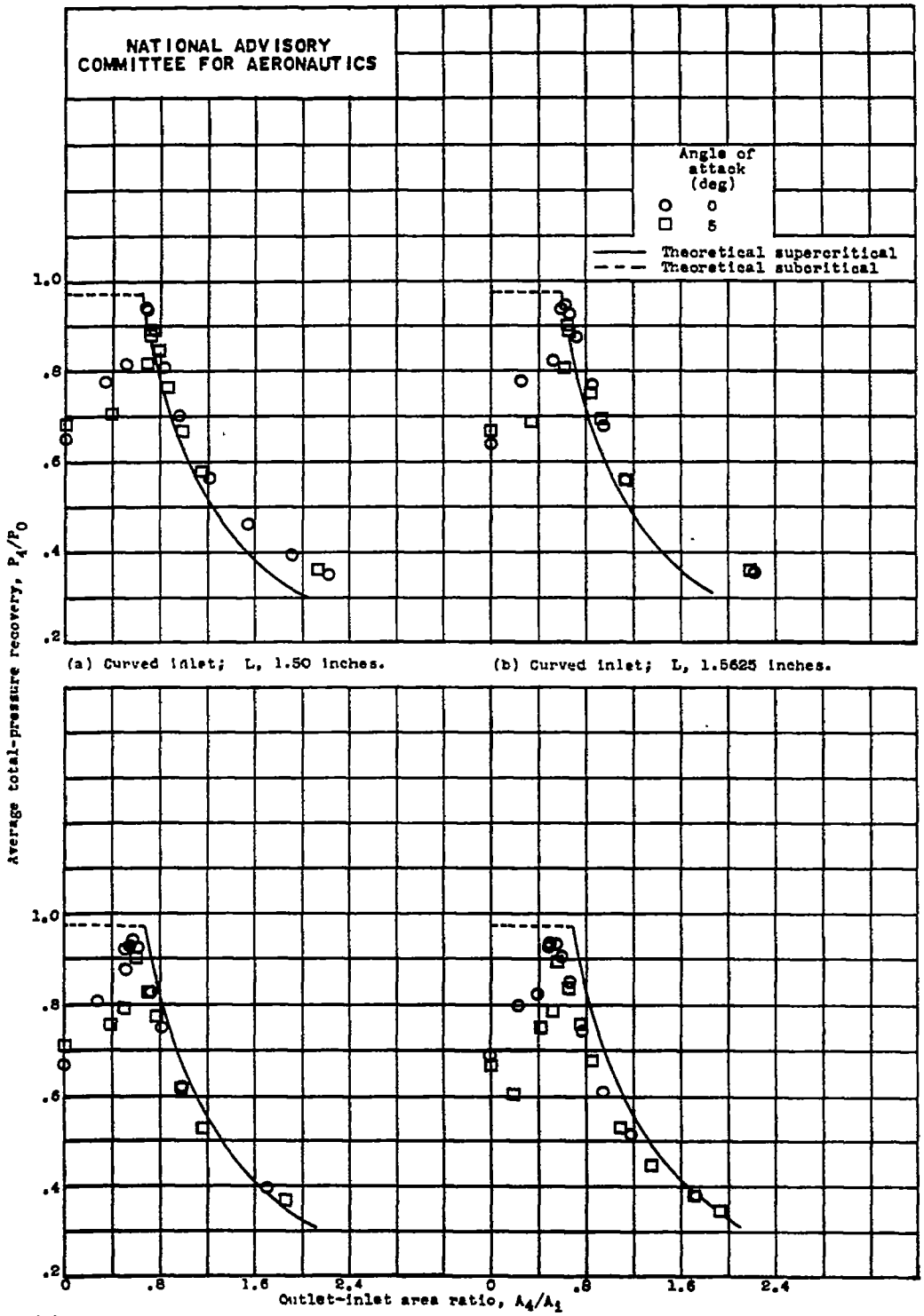

(a) Curved inlet; L, 1.50 inches. (b) Curved inlet; L, 1.5625 inches.

(c) Straight inlet; L, 1.6875 inches. (d) Straight inlet; L, 1.75 inches.

Figure 8.- Effect of angle of attack on total-pressure recovery obtained with four configurations of the 30-60 cone.

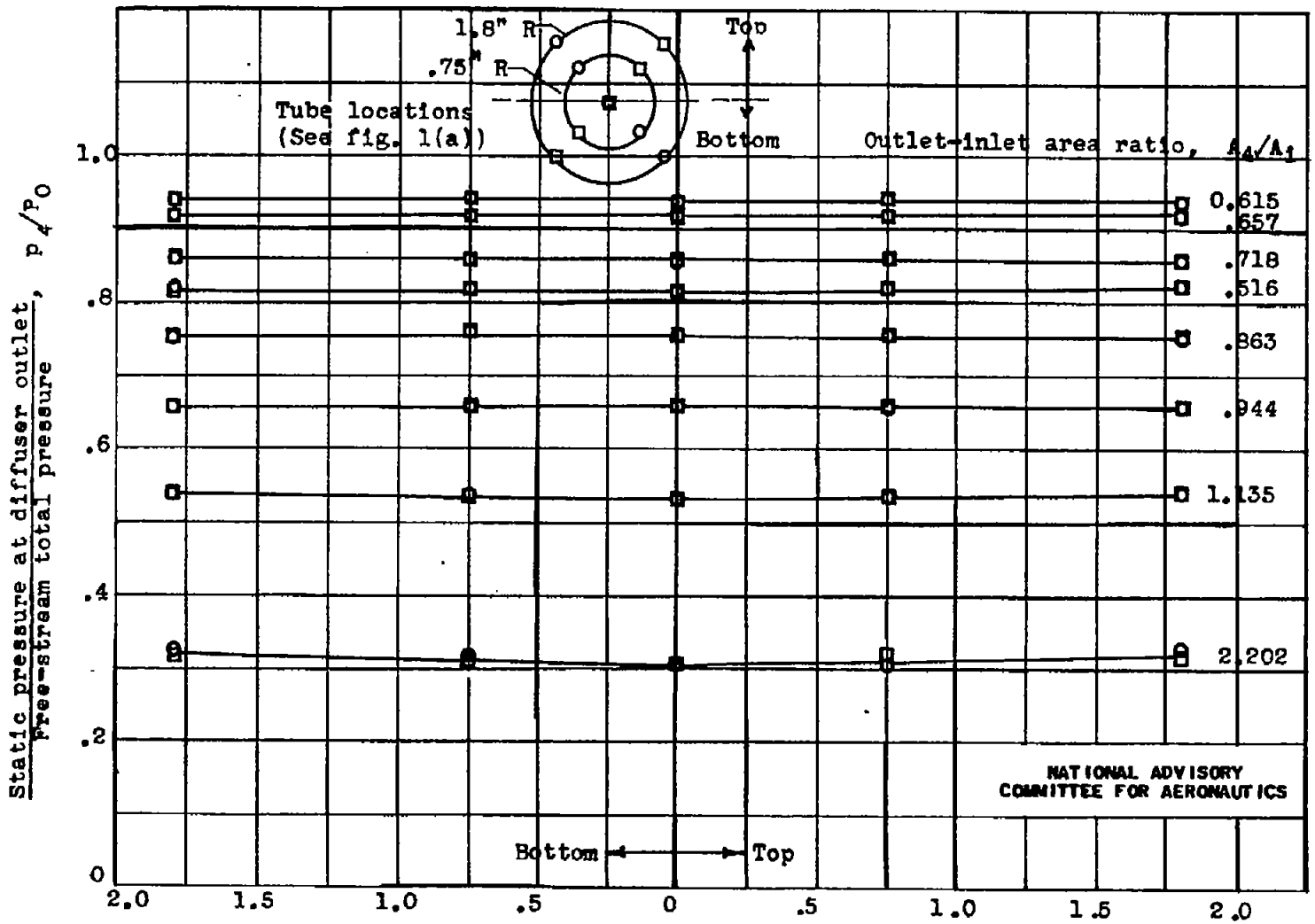

(a) Static-pressure distribution at 0° angle of attack.

Figure 9.- Pressure distributions across diffuser outlet for configuration giving best efficiency. 30-60 cone; curved inlet; tip projection, 1.5625 inches.

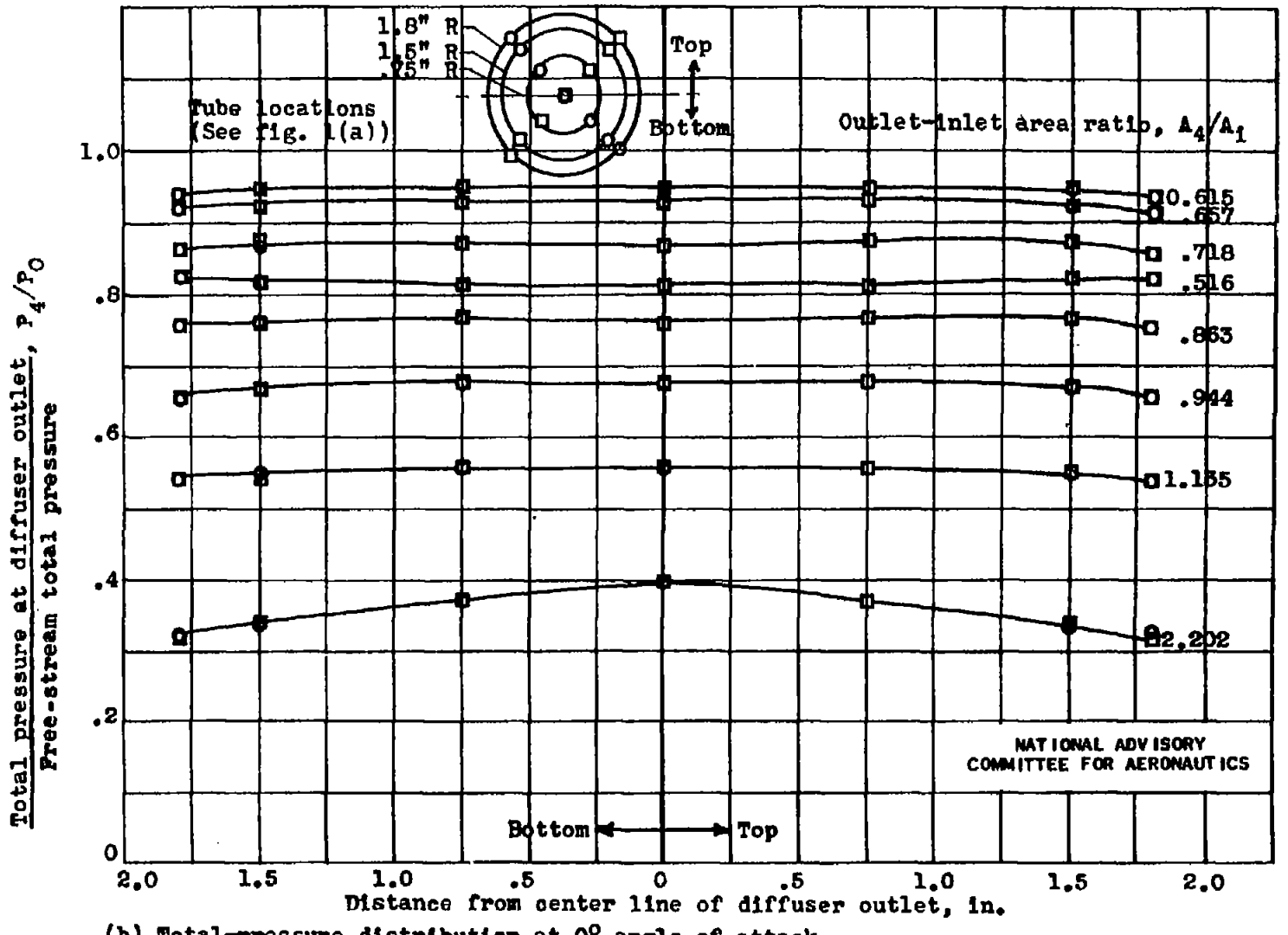

(b) Total-pressure distribution at 0° angle of attack.

Figure 9.- Continued. Pressure distributions across diffuser outlet for configuration giving best efficiency. 30-60 cone; curved inlet; tip projection, 1.5625 inches.

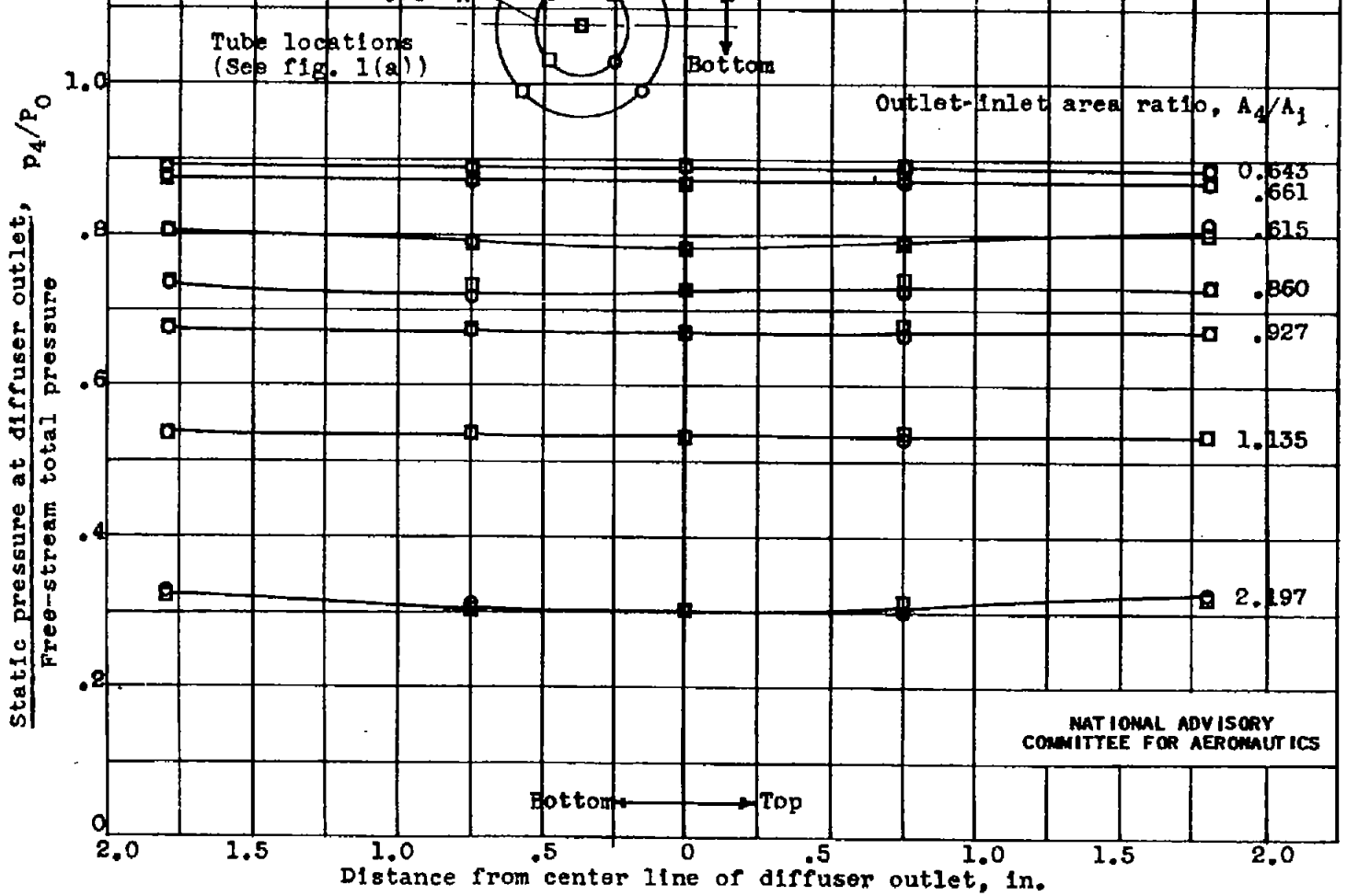

(c) Static-pressure distribution at 5° angle of attack.

Figure 9.- Continued. Pressure distributions across diffuser outlet for configuration giving best efficiency. 30-60 cone; curved inlet; tip projection, 1.5625 inches.

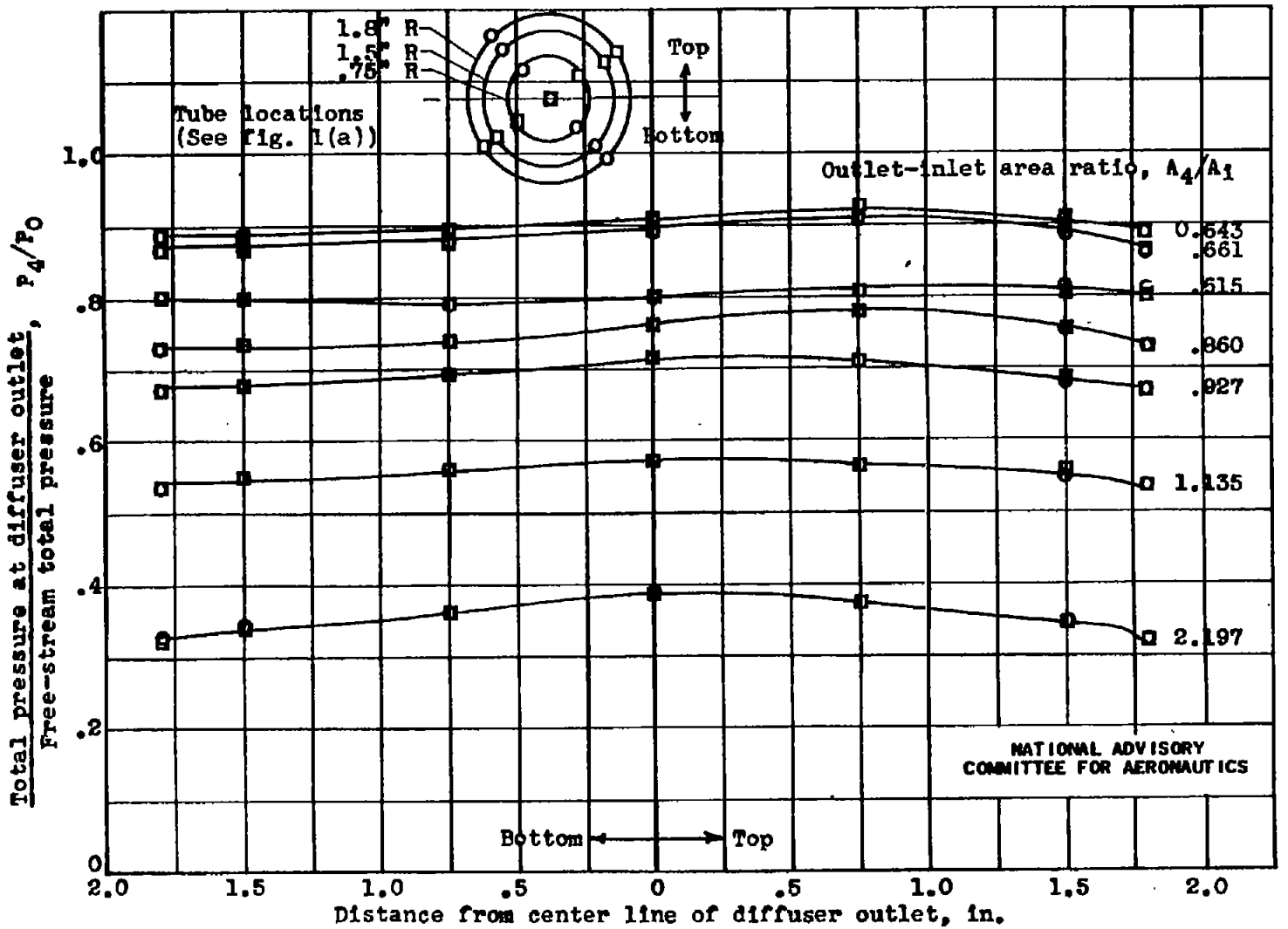

(d) Total-pressure distribution at 5° angle of attack.

Figure 9.- Concluded. Pressure distributions across diffuser outlet for configuration giving best efficiency. 30-60 cone; curved inlet; tip projection, 1.5625 inches.

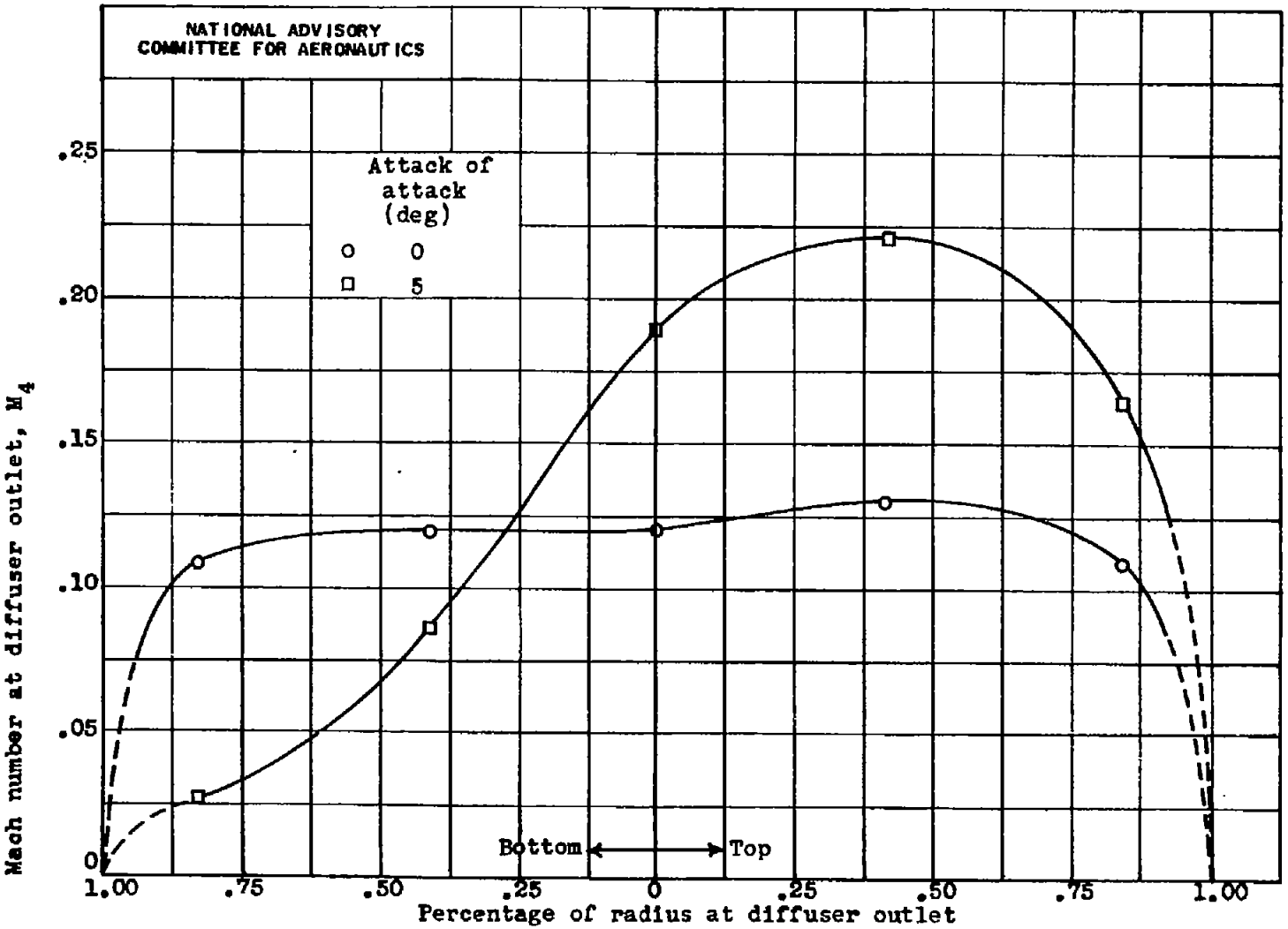

Figure 10.- Mach-number distribution at diffuser outlet at angles of attack of 0° and 5° for configuration giving best efficiency. 30-60 cone; curved inlet; L, 1.5625 inches.

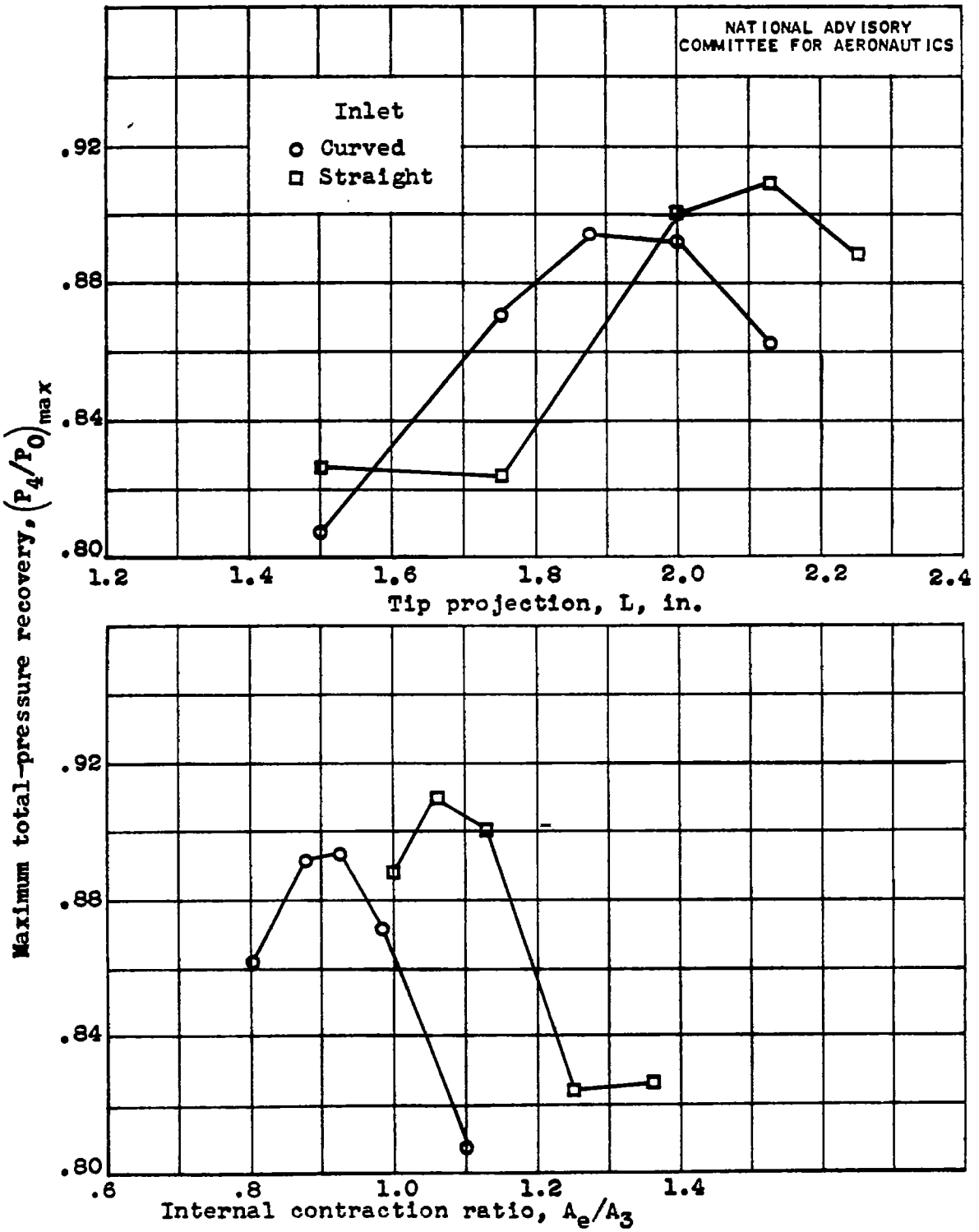

(a) 20-40 cone.

Figure 11.- Variation of maximum total-pressure recovery with tip projection and internal contraction ratio.

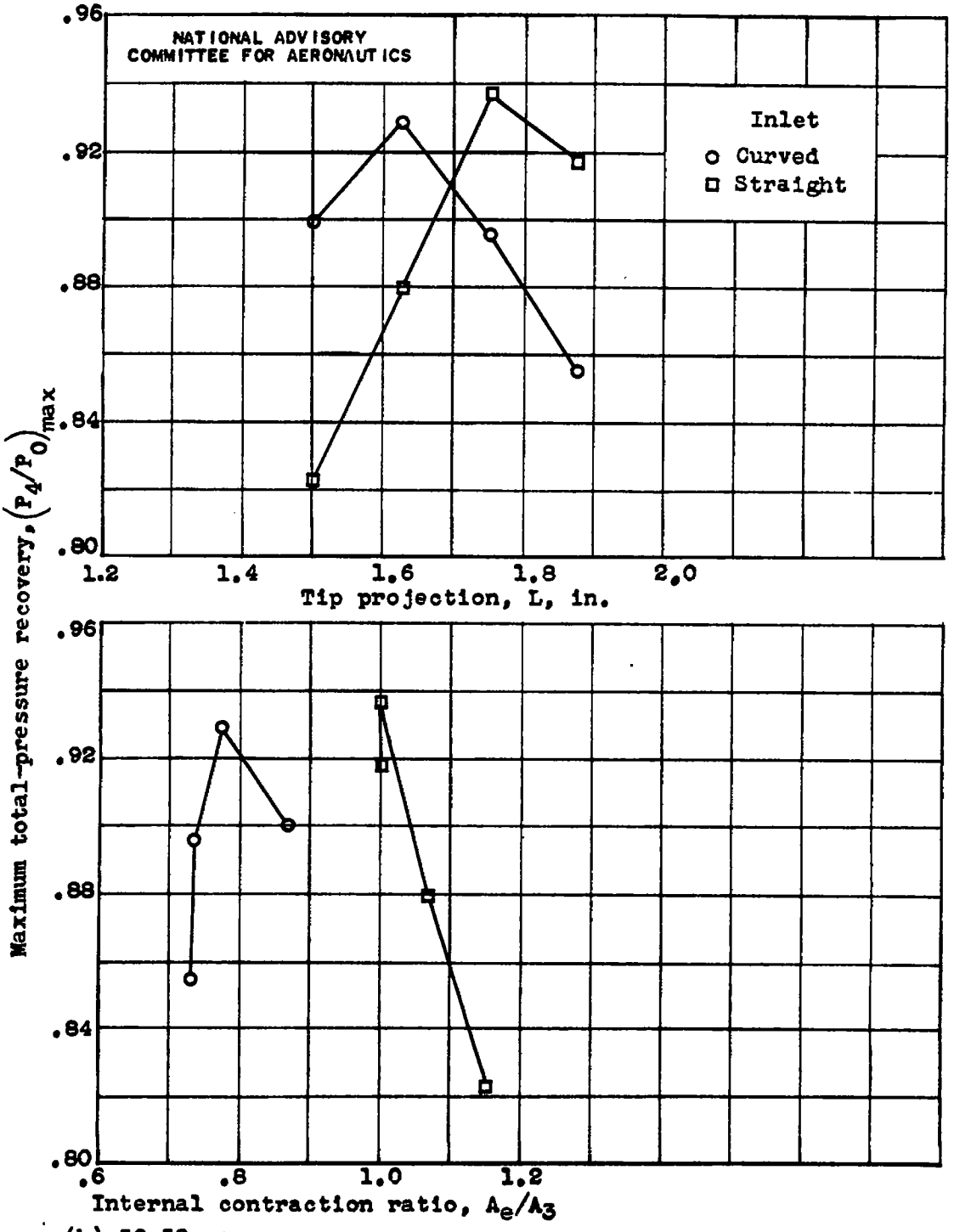

(b) 30-50 cone.

Figure 11.- Continued. Variation of maximum total-pressure recovery with tip projection and internal contraction ratio.

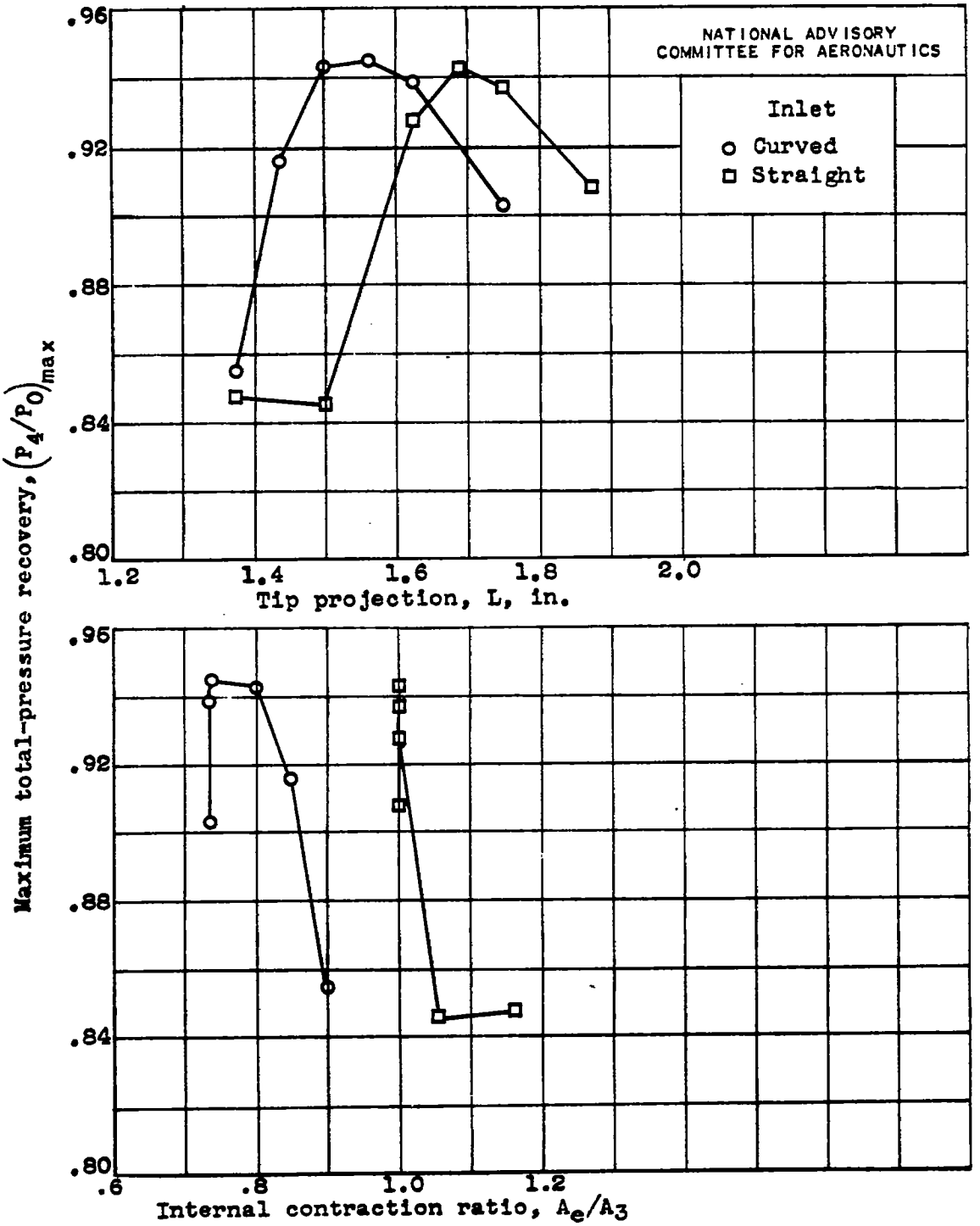

(c) 30-60 cone.

Figure 11.- Continued. Variation of maximum total-pressure recovery with tip projection and internal contraction ratio.

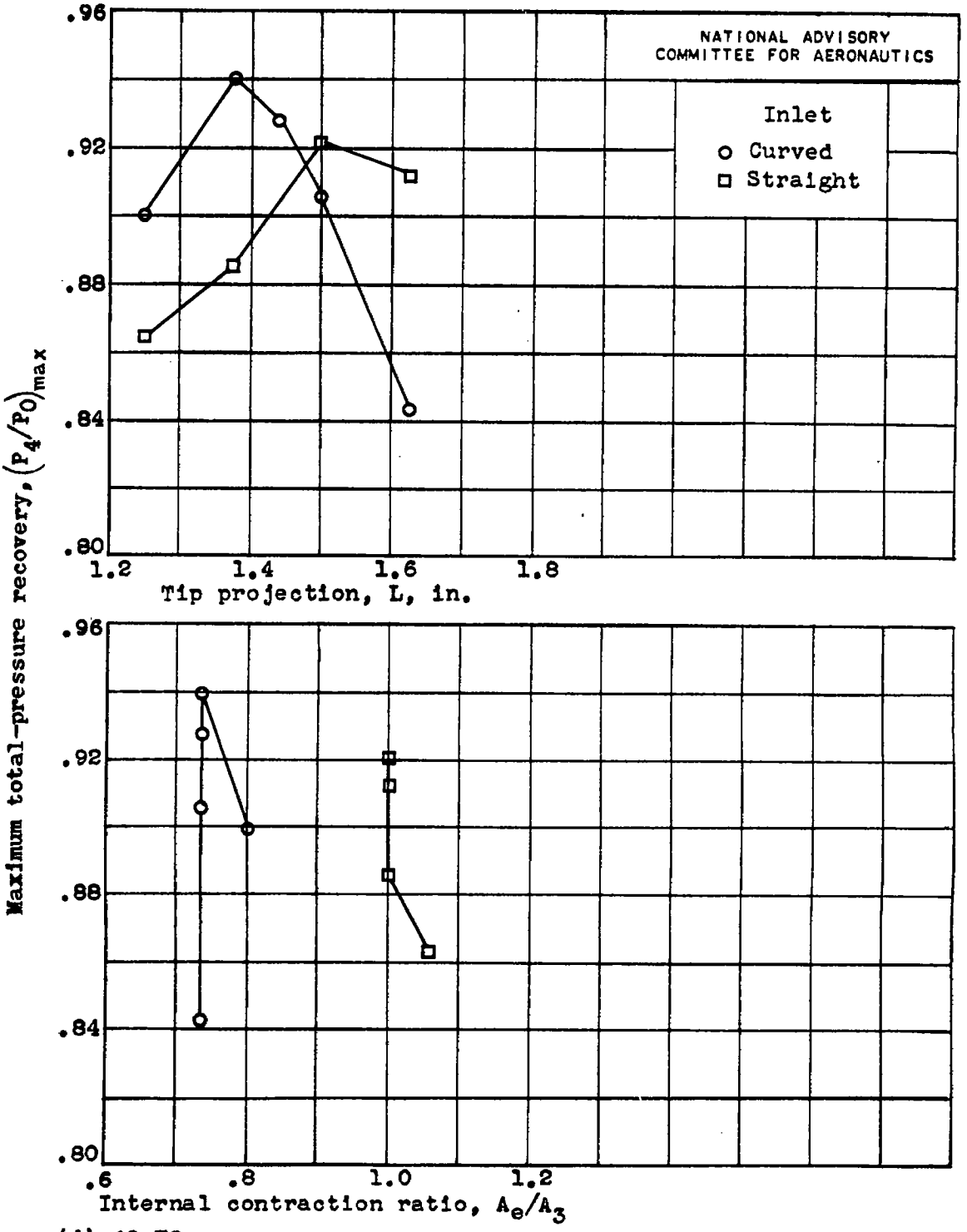

(d) 40-70 cone.

Figure 11.- Concluded. Variation of maximum total-pressure recovery with tip projection and internal contraction ratio.